Influence of particle size and type on 231Pa and 230Th simulation with a global coupled biogeochemical-ocean general circulation model: A first approach

J. C. Dutay, F. Lacan, M. Roy-Barman, L. Bopp

Geochemistry Geophysics Geosystems G3
AN ELECTRONIC JOURNAL OF THE EARTH SCIENCES
Published by AGU and the Geochemical Society

Article
Volume 10, Number 1
31 January 2009
Q01011, doi:10.1029/2008GC002291
ISSN: 1525-2027

Influence of particle size and type on ^{231}Pa and ^{230}Th simulation with a global coupled biogeochemical-ocean general circulation model: A first approach

J.-C. Dutay
LSCE, IPSL, Laboratoire CEA, UVSQ, CNRS, F-91191 Gif sur Yvette, France
(jean-claude.dutay@lsce.ipsl.fr)

F. Lacan
LSCE, IPSL, Laboratoire CEA, UVSQ, CNRS, F-91191 Gif sur Yvette, France

Now at LEGOS, F-31401 Toulouse CEDEX 9, France

M. Roy-Barman and L. Bopp
LSCE, IPSL, Laboratoire CEA, UVSQ, CNRS, F-91191 Gif sur Yvette, France

[1] The oceanic distributions of ^{231}Pa and ^{230}Th are simulated with the global coupled biogeochemical-ocean general circulation model NEMO-PISCES. These natural nonconservative tracers, which are removed from the water column by reversible scavenging processes onto particles, have been used to study modern and past ocean circulation. Our model includes three different types of particles: particulate organic matter (POM), calcium carbonate ($CaCO_3$), and biogenic silica (BSi). It also considers two particle classes: small particles (POM) that sink slowly (3 m/d) and large particles (POM, $CaCO_3$, BSi) that sink much more rapidly (50 m/d to 200 m/d) in the water column. ^{231}Pa and ^{230}Th are simulated with a reversible scavenging model that uses partition coefficients between dissolved and particulate phases that depend on particle type and size. Model results are then compared with ^{231}Pa and ^{230}Th observations in the water column and modern sediments. A preliminary evaluation of the particle fields simulated by the PISCES model has revealed that particle concentrations are reasonable at the surface but largely underestimated in the deep ocean. Largely to compensate for this, we find it necessary to use partition coefficients that vary as a function of particle size by significantly more that observed to obtain relatively realistic results. In the water column, ^{231}Pa and ^{230}Th fluxes are mainly controlled by the slowly sinking particles and partition coefficients need to be parameterized as a function of particle flux, as suggested by observations. Considering discrepancies between the modeling particle fields and those observed, we were forced to use exaggerated values for partition coefficients in order to get realistic tracer distributions. These ^{231}Pa and ^{230}Th simulations have provided an opportunity to propose some future developments of the PISCES model, in order to make progress in the simulation of trace elements. Assigning calcium carbonate, biogenic silica, and aluminosilicates to the small particle pool represents a credible approach to increase its concentration and subsequently simulate realistic tracer distributions in the water column using reasonable values for the partition coefficients, as well as a realistic fractionation in the sediments at all depths.

Components: 11,382 words, 11 figures, 1 table.

Keywords: modeling; trace element.

Index Terms: 4805 Oceanography: Biological and Chemical: Biogeochemical cycles, processes, and modeling (0412, 0414, 0793, 1615, 4912); 4808 Oceanography: Biological and Chemical: Chemical tracers.

Received 4 June 2008; **Revised** 20 October 2008; **Accepted** 20 November 2008; **Published** 31 January 2009.

Dutay, J.-C., F. Lacan, M. Roy-Barman, and L. Bopp (2009), Influence of particle size and type on ^{231}Pa and ^{230}Th simulation with a global coupled biogeochemical-ocean general circulation model: A first approach, *Geochem. Geophys. Geosyst.*, *10*, Q01011, doi:10.1029/2008GC002291.

1. Introduction

[2] The ocean has a great capacity to store and transport heat, water, and radiatively active gases around the globe and to exchange these with the atmosphere. Accordingly, changes in ocean circulation are now widely thought to be involved in past climate change [*Duplessy et al.*, 1988; *Rahmstorf*, 2002; *Curry and Oppo*, 2005]. Constraining the past oceanic variability and understanding the ocean carbon cycle and the role of the thermohaline circulation in the regulation of the Earth's climate are necessary to improve our understanding of the climate system. To address these questions, we must be able to evaluate the role of ocean circulation in transporting not only heat and salt but also dissolved and particulate compounds that interact with the marine carbon cycle (nutrients, dissolved and particulate inorganic carbon, dissolved and particulate organic carbon).

[3] In paleoceanography, reconstructions are performed via the use of proxies that must be calibrated in the modern ocean. Each given proxy is always sensitive to a different set of variables, and reconstructions must exploit a multiproxy approach. For example, reconstructions of the past thermohaline circulation requires the unraveling of the effects of changing circulation and ocean chemistry on proxies such as δ^{13}C [*Charles and Fairbanks*, 1992] and Cd/Ca [*Lea*, 1995]. The considerable analytical progress achieved during the last decades now permits the use of nonconservative trace elements, such as ^{230}Th and ^{231}Pa, for studying modern and past changes in ocean circulation [*McManus et al.*, 2004; *Gherardi et al.*, 2005] and biological productivity [*Kumar et al.*, 1993, 1995; *Bradtmiller et al.*, 2007].

[4] ^{231}Pa (32.5 ka half-life) and ^{230}Th (75.2 ka half-life) are natural radioisotopes produced in the ocean by α decay of ^{235}U and ^{234}U, respectively [*Henderson and Anderson*, 2003]. Because the activity of U is approximately uniform in the ocean, ^{231}Pa and ^{230}Th are produced at a relatively constant rate ($\beta^{Pa} = 2.33 \times 10^{-3}$ dpm m^{-3} a^{-1}, $\beta^{Th} = 2.52 \times 10^{-2}$ dpm m^{-3} a^{-1}) with a production ratio (β^{Pa}/β^{Th}) of 0.093 [*Henderson and Anderson*, 2003]. They are both scavenged rapidly onto marine particles that subsequently transport them toward the sediment on a timescale of 20–40 years for ^{230}Th and of 80–200 years for ^{231}Pa [*Yu et al.*, 1996]. When particulate transport balances in situ production, the activity of ^{230}Th and ^{231}Pa should increase approximately linearly with depth [*Bacon and Anderson*, 1982; *Roy-Barman et al.*, 1996]. Therefore any deviations from the linear profile indicate that ocean currents have transported ^{230}Th and ^{231}Pa away from their production sites [*Moran et al.*, 2001; *Rutgers van der Loeff and Berger*, 1993]. Because ^{230}Th has a low residence time, most of its in situ production is exported vertically by marine particles. Moored sediment traps can then be calibrated by comparing the ^{230}Th$_{xs}$ inventories ("^{230}Th$_{XS}$" represents the ^{230}Th produced in seawater and scavenged by marine particles as opposed to the ^{230}Th carried by lithogenic particles) collected by traps with the in situ production above the traps [*Scholten et al.*, 2001]. Present ocean transport can then be estimated by observing their effect on dissolved ^{230}Th$_{xs}$ and ^{231}Pa$_{xs}$ profiles [*Moran et al.*, 2002].

[5] Because ^{231}Pa is less sensitive to particle scavenging than ^{230}Th, the ^{231}Pa/^{230}Th ratio in oceanic sediments reflects the relative importance of advection-diffusion and particle scavenging on their transport and is therefore a potential means by which to reconstruct past ocean circulation. Using this tool, recent work suggests a complete shut down of the NADW circulation during the H1 Heinrich event [*McManus et al.*, 2004; *Gherardi et al.*, 2005]. Using ^{231}Pa and ^{230}Th to study

modern and past ocean circulation requires better understanding and constraints on the processes that control their distribution. However, our knowledge of the interactions between these tracers and marine particles remains limited and the detailed processes driving ^{230}Th and ^{231}Pa behavior are largely unknown. At present, there is still an open debate concerning the phase(s) that carry ^{230}Th and ^{231}Pa in the oceans particulate matter [*Luo and Ku*, 1999; *Chase et al.*, 2002; *Luo and Ku*, 2004; *Chase and Anderson*, 2004; *Roy-Barman et al.*, 2005; *Siddall et al.*, 2005]. For example, ^{230}Th-based trapping efficiencies as low as 10–30% clearly demonstrate that Th-bearing phases can be undercollected in certain conditions [*Scholten et al.*, 2001]. It is likely that $^{230}Th_{xs}$ is scavenged onto fine particles before being transferred to large rapidly sinking particles. A preferential undertrapping of small slowly sinking particles produces a loss of $^{230}Th_{xs}$ but may not affect rapidly sinking aggregates carrying particulate organic matter (POM) and $CaCO_3$. In this case, POM and $CaCO_3$ fluxes corrected for trapping efficiency are overestimated. On the other hand, if small particles are packaged as fecal pellets or embedded in large aggregates, the ^{230}Th calibration is relevant for POM and $CaCO_3$.

[6] Numerical models offer a unique opportunity to study the processes that control the oceanic distribution of trace elements and their isotopes. Models are also particularly important in separating and quantifying the different processes that control the distribution of these elements and isotopes. To study the cycle of such trace elements models require several components: a dynamical model to provide the advective and mixing processes that redistribute the tracer within the ocean, a biological model to generate the particle distributions and fluxes that scavenge the tracers in the ocean, and finally a scavenging model that simulates the exchange of tracer between the dissolved and particulate phases (adsorption, desorption, remineralization, sinking). Thus far, few global modeling studies have considered nonconservative trace elements. ^{231}Pa and ^{230}Th have been simulated in models of intermediate complexity (EMIC 2.5D) [*Marchal et al.*, 2000], (EMIC 3D) [*Siddall et al.*, 2005, 2007], and in the Hamburg Large-Scale Geostrophic model [*Henderson et al.*, 1999; *Heinze et al.*, 2006]. While these pioneer studies undertook a wide variety of sensitivity tests to examine the relative impacts of transport and distinct particle affinities (e.g., for POM, CaCO3, SiO2, dust) on the scavenging and fractionation of ^{231}Pa and ^{230}Th, such simplified models necessarily underestimate the potential complexity of the system. For instance, all of these simulation used an annual average particle sinking velocity on the order of 3 m/d, which is consistent with apparent sinking velocities that are estimated from ^{230}Th observations [*Krishnaswami et al.*, 1981; *Bacon and Anderson*, 1982; *Rutgers van der Loeff and Berger*, 1993; *Scholten et al.*, 1995], while field observations clearly indicate that some particles sink with velocities that can be typically one or two orders of magnitude higher [*Berelson*, 2001; *Stemmann et al.*, 2004; *Venchiarutti et al.*, 2008]. Taking into account both rapidly and slowly sinking particles is extremely important in accounting for some features of Pa-Th fractionations that are clearly inconsistent with a single class of small sinking particles. For example, in the southern sector of the Atlantic Ocean, large sinking particles have a much higher ^{231}Pa/^{230}Th ratio than the deep suspended particles [*Walter et al.*, 2001]. While the sediment ^{231}Pa/^{230}Th budget in this region is primarily controlled by scavenging from the standing stock of deep suspended particles, the contribution of the large sinking particles to the Pa budget cannot be neglected. In the southern sector of the Pacific Ocean, the strong Pa flux to the sediment is not associated with a depletion in dissolved ^{231}Pa throughout the entire water column [*Chase et al.*, 2003]. Instead, the strong Pa flux is due to ^{231}Pa scavenging in the surface waters by diatoms. Such a process is clearly inconsistent with the simple reversible exchange of the *Bacon and Anderson* [1982] model. Furthermore, diatom-driven ^{231}Pa/^{230}Th fractionation is also observed in the equatorial Pacific [*Chase et al.*, 2002; *Bradtmiller et al.*, 2007]. Variability in shallow versus deep scavenging has also been reported for Th [*Coppola et al.*, 2006] and Nd [*Jeandel et al.*, 1995] isotopes. Understanding scavenging processes is not only important in modeling dissolved Pa and Th, it is a means by which the relative role of small and large particles in the transport of particulate material can be determined as the depth of formation of the particles can be traced through their isotopic signature [*Coppola et al.*, 2006]. Differential scavenging is also of critical importance when using the ^{231}Pa/^{230}Th ratio in the sediment as paleocirculation tracer in order to determine if the sediment records whether the ^{231}Pa/^{230}Th of the bottom water mass in areas where high advection sinking particles pick up the advected Pa/Th signature or if it integrates a signal over the whole water column when the advection is low [*Gherardi et al.*, 2005; *Thomas et al.*, 2006].

[7] In this paper, ^{231}Pa and ^{230}Th distributions are simulated for the first time with a coupled biogeochemical/ocean general circulation model (OGCM). The dynamical component is NEMO [*Madec et al.*, 1998], and the biogeochemical component is the Pelagic Interactions Scheme for Carbon and Ecosystem Studies (PISCES) model [*Aumont and Bopp*, 2006]. PISCES was developed initially to address questions mainly regarding air-sea carbon fluxes and marine ecosystem variability over interannual to millennial timescales [*Bopp et al.*, 2003].

[8] Using this complex biogeochemical model to simulate the trace elements distribution is motivated by the desire of a common tool for both carbon cycle and trace elements research. Following this joint approach reinforces the links between the two communities and should provide future benefits for both disciplines. Because PISCES is designed with two size classes of particles with different sinking velocities, we can address herein the role of fast-sinking particles in shaping ^{231}Pa and ^{230}Th distributions. This was not possible in previous global modeling studies, in which a unique settling velocity for particles was used.

[9] This paper has two objectives: (1) using ^{231}Pa and ^{230}Th simulations to provide an additional evaluation of the particles fields generated by the PISCES model and (2) using ^{231}Pa and ^{230}Th simulations to acquire additional knowledge on the links between these trace isotopes elements and ocean circulation/particle dynamics in the past and modern ocean.

2. Model Description and Observations

2.1. Physical Model

[10] The physical model is the Nucleus for European Modeling of the Ocean (NEMO) model, which is based on the ORCA2 global configuration of the ocean model OPA [*Madec et al.*, 1998]. The nominal horizontal resolution is 2° by 2° × cos(latitude), with a meridional resolution enhanced to 0.5° near the equator. The mesh overcomes singularities near the North Pole by getting two inland poles on the northern hemisphere. The model has 30 vertical layers increasing from 10 m resolution at the surface to 500 m resolution at the bottom. The upper boundary uses a free surface formulation [*Roullet and Madec*, 2000]. The surface mixed layer is modeled by a turbulent kinetic energy (TKE) closure [*Blanke and Delecluse*, 1993]. Lateral diffusion is performed along local isopycnal surfaces, and the eddy induced velocity parameterization of *Gent and McWilliams* [1990] is applied. The flow of deep water along bathymetry is represented using the bottom boundary layer (BBL) parameterization proposed by *Beckmann and Döscher* [1997]. The model is coupled with the dynamical-thermodynamical sea ice model LIM (Louvain-la-Neuve sea-ice model) [*Fichefet and Morales Masqueda*, 1997]. At the surface the model is forced by fluxes of heat and freshwater computed by means of bulk formulae [*Timmermann et al.*, 2005] and daily wind stress based on ERS satellite for the Tropics and NCEP/NCAR near the poles. Surface salinity is readjusted to the monthly WA01 data set [*Conkright et al.*, 2002] with a timescale of 40 days to avoid model drift. The OPA model is widely used in oceanic and climate studies (http://www.lodyc.jussieu.fr/NEMO/general/biblio_new/en/one/bibnemomaf01.html). The evaluation of its circulation with geochemical tracers (CFCs, ^{14}C, natural^{3}He) during the Ocean Carbon Model Intercomparison Project (OCMIP) demonstrated that even though it has the classical default associated with coarse resolution models (crude representation of bottom water formation, sluggish deep western boundary current (DWBC)...), it produces a reasonable thermohaline structure that is completely acceptable to perform biogeochemical studies with a global meridional overturning circulation (MOC) of 17.5 Sv for NADW and 11.8 Sv for AABW [*Dutay et al.*, 2002, 2004; *Matsumoto et al.*, 2004; *Arsouze et al.*, 2007; *Doney et al.*, 2004].

2.2. Ocean Biogeochemical Model

[11] We use the Pelagic Interaction Scheme for Carbon and Ecosystem Studies (PISCES) biogeochemical model. The model simulates the biogeochemical cycles of carbon, oxygen and five nutrients (nitrate, ammonium, phosphate, silicate, and iron) that can limit phytoplankton growth. Two phytoplankton groups (nanophytoplankton and diatoms) and two zooplankton groups (microzooplankton and mesozooplankton) are represented. For all species, constant Redfield ratios are imposed for C/N/P. There are three nonliving compartments: semilabile dissolved organic carbon (DOC) and small and large particles. The two particle classes differ by their sinking velocities and composition: The sinking velocity for small particle (w_s) is 3 m/d, while for large particles it linearly increases between 50 m/d at the surface to up to 300 m/d at the bottom of the ocean. Small particles consist of particulate organic carbon (POM), with a size between 2 and 100 μm. Their

corresponding settling velocities (3 m/day) have been estimated via a relation that represents the sinking speed as a function of size, as proposed by *Kriest* [2002]. The large particulate pool includes particulate organic carbon (POMb), but also biogenic silica (BSi) and carbonate ($CaCO_3$) that sink faster due to their excess density that generates higher settling rates according to the Stokes Law [*Gehlen et al.*, 2006]. The content of the particulate pools is controlled by mortality, grazing, and mineralization, and the two POC classes interact via the processes of aggregation and disaggregation (see Appendix A for more details). A detailed description of the model including model equations and parameterization is available as supplementary material in the work of *Aumont and Bopp* [2006]. This simplified description of the marine particles (particularly the small particle pool) gives a major role to the particulate organic matter on the scavenging of dissolved radionuclide by the small particle pool. This is consistent with recent advances on the thorium speciation that considers that scavenging of dissolved Th is largely controlled by organic compounds [*Guo et al.*, 2002; *Santschi et al.*, 2006].

2.3. Reversible Scavenging Model

[12] The observed increase of dissolved and particulate ^{231}Pa and ^{230}Th activities with depth implies a continuous and reversible exchange between the dissolved and particulate phase as the particles sink through the water column [*Bacon and Anderson*, 1982; *Nozaki et al.*, 1981]. For our simulations, we have followed the approach proposed by *Henderson et al.* [1999] and *Siddall et al.* [2005], which considers that the partition between dissolved and particulate phase is in equilibrium, as suggested by observations [*Bacon and Anderson*, 1982; *Moore and Hunter*, 1985; *Roy-Barman et al.*, 1996]. In this approach the ratio between dissolved (A_d) and particulate (A_p) activities is set by equilibrium partition coefficients, K_d, defined as:

$$K_d^i = \frac{A_p^i}{A_d^i C_p}$$

where C_p is the mass of particle per mass of water, and superscript "i" refers to the type of particle, i.e., particulate organic carbon (POMs, POMb), biogenic silica (BSi), and calcite ($CaCO_3$). The lithogenic contribution (dust) is neglected in our simulations.

[13] The total activities of the tracers $A_T = A_d + A_p$ are transported in the model following the continuity equation:

$$\frac{\partial A_T^i}{\partial t} = \beta_i - \lambda^i A_T^i - \frac{\partial\left(w_s A_{poms}^i\right)}{\partial z} - \frac{\partial\left(w_b A_{pb}^i\right)}{\partial z} + [Advection - Diffusion]\left(A_T^i\right)$$

where β is the production rate, λ is the radioactive decay, and A_{POMs} and A_{pb} represent respectively activities for small particle (POMs) and the large particle pool (POMb, BSi, $CaCO_3$). These latter quantities are diagnosed from the total and dissolved activities using the partition coefficient:

$$A_T = A_{pocs} + A_{pb} + A_d = \left(K_{Dpoms}C_{poms} + K_{Dpomb}C_{pomb} + K_{DCaCO_3}C_{CaCO_3} + K_{DBSi}C_{BSi} + 1\right).A_d$$

$$A_{poms} = \frac{K_{Dpoms}C_{poms}}{\left(K_{Dpoms}C_{poms} + K_{Dpomb}C_{pomb} + K_{DCaCO_3}C_{CaCO_3} + K_{DBSi}C_{BSi} + 1\right)}A_T$$

$$A_{pb} = \frac{K_{pomb}C_{pomb} + K_{CaCO_3}C_{CaCO_3} + K_{bSi}C_{BSi}}{\left(K_{Dpoms}C_{poms} + K_{Dpomb}C_{pomb} + K_{DCaCO_3}C_{CaCO_3} + K_{DBSi}C_{BSi} + 1\right)}A_T$$

This approach confers a great advantage in that only two tracers are transported in our simulations (total activities of ^{231}Pa and ^{230}Th). Moreover the simulations are performed "off-line" using seasonal fields of the three velocity components, mixing coefficients and particle concentration for each particle type previously calculated with the model NEMO-PISCES. This overall method requires considerably lower computational cost which allowed us to simulate ^{231}Pa and ^{230}Th with an OGCM and to perform some sensitivity tests on the values of the partition coefficients.

[14] The values of the partition coefficients for ^{231}Pa and ^{230}Th as a function of particle type are weakly constrained by observations, and an uncertainty of at least one order of magnitude remains. Moreover, the debate regarding the nature of the phase that scavenges these tracers in the ocean remains active [*Luo and Ku*, 1999; *Chase et al.*, 2002; *Luo and Ku*, 2004; *Chase and Anderson*, 2004; *Roy-Barman et al.*, 2005; *Li*, 2005; *Siddall et al.*, 2005]. Taking into account the limited number of simulations that can be performed with our model, we have used insights gained from previous modeling studies to design our experiments. We have performed five simulations with different sets of partition coefficients (Table 1). The first experiment (Exp 1) makes use of the

Table 1. Description of the Simulations[a]

	Exp.1	Exp. 2	Exp. 3	Exp. 4	Exp. 5
K(POMs) Pa	1.e + 7	1.e + 9	1.e + 9 * F (Cp)	1.e + 9	2.e + 8
K(POMs) Th	1.e + 7	1.e + 9	1.e + 9 * F(Cp)	1.e + 9	1.e + 9
K(POMb) Pa	1.e + 7	1.e + 6	1.e + 6	1.e + 6	1.e + 6
K(POMb) Th	1.e + 7	1.e + 6	1.e + 6	1.e + 6	1.e + 6
K(BSi) Pa	0.17.e + 7	0.17.e + 7	0.17.e + 7	0.17.e + 7	0.17.e + 7
K(BSi) Th	0.05.e + 7	0.05.e + 7	0.05.e + 7	0.005.e + 7	0.05.e + 7
K($CaCO_3$) Pa	0.025e + 7	0.025e + 7	0.025e + 7	0.025e + 7	0.025e + 7
K($CaCO_3$) Th	1.e + 7	1.e + 7	1.e + 7	1.e + 7	1.e + 7

[a] Exp. is experiment. F (Cp) = EXP ((−4./9.) × log(Cp) is a function representing covariation of Kd with particle concentration estimated from *Honeyman et al.* [1988].

partition coefficients based on *Chase et al.* [2004] that were used in the standard simulation of *Siddall et al.* [2005]. It has identical values for ^{231}Pa and ^{230}Th for particulate organic carbon (POMb, POMs), but introduces a large fractionation between Th and Pa for carbonate (a factor 40), whereas the partition coefficient for ^{230}Th is slightly less than for ^{231}Pa (a factor 3) for opal, as suggested by *Chase et al.* [2004]. The strategy for defining the partition coefficients of the other experiments relied on observations, as well as the understanding gained from our sensitivity experiments. Exp 2 has partition coefficients that vary with both particle composition and particle flux, with higher K_d values for the small particles and lower values for large rapidly sinking particles, as suggested by *Chase et al.* [2004]. Exp 3 has the same partition coefficient as Exp 2 but includes a Kd that varies with the particle mass for small particles as suggested by *Honeyman et al.* [1988] and tested in a model by *Henderson et al.* [1999]. Exp 4 and 5 are sensitivity tests around experiment 2, where the value of the Kd are reduced on BSi for ^{230}Th(exp4) and on POM for ^{231}Pa (exp 5).

2.4. Observations

[15] Water column data of dissolved, particulate, and total (unfiltered) ^{230}Th and ^{231}Pa known to us were compiled. We included published [*Marchal et al.*, 2007] and unpublished water column data from R. Francois. For the sediments, we used the Holocene ^{231}Pa/^{230}Th data set compiled by G. Henderson (http://www.earth.ox.ac.uk/%7Egideonh/index.html).

3. Results and Discussion

3.1. Distributions of Particles

[16] We first provide a description and evaluation of the particle fields generated by the OPA-PISCES model in order to facilitate the interpretation of the tracers' simulations. A comparison of the vertical fluxes predicted by this model with sediment traps data can be found in the work of *Gehlen et al.* [2006]. This comparison reveals that OPA-PISCES model predicts a wider spread in POM fluxes between 1000 and 2000 m than is present in the data set, with a tendency toward overestimation. Modeled deep-water fluxes are of the right order of magnitude, although the modeled variability below 3800 m is underestimated. However, in modeling reactive species such as Pa and Th, not only is the particles flux important, but the standing stock of particle mass in the oceans is also an essential factor. The annually averaged surface distribution of particle concentrations generated by the PISCES model is shown in Figure 1. The surface total concentration of particles is dominated by small particles. All types of particles show maximum concentrations in the regions of high productivity: the high latitudes, the equatorial Pacific Ocean, or coastal upwelling regions such as along the eastern boundary of the South Pacific and south Atlantic Oceans. The highest surface concentrations are obtained for small particles (POMs), which also exhibit the weakest spatial gradients. For large particles, surface concentrations tend to be at least one order of magnitude lower than those simulated for small particles, except for BSi in the Southern Ocean. For large particles, the spatial gradients are more pronounced, with lower relative values in the regions of low productivity (subtropical gyres). The global zonally averaged concentration of particles as a function of depth (Figure 2) allows us to analyze the vertical structure of particle distributions, which is an important factor controlling the downward flux of particle reactive elements in the oceans. The small particle (POMs) distribution exhibits the most pronounced decrease with depth (up to 3 orders of magnitude), due to rapid remineralization and aggregation. All types of large particles display more moderate vertical variations

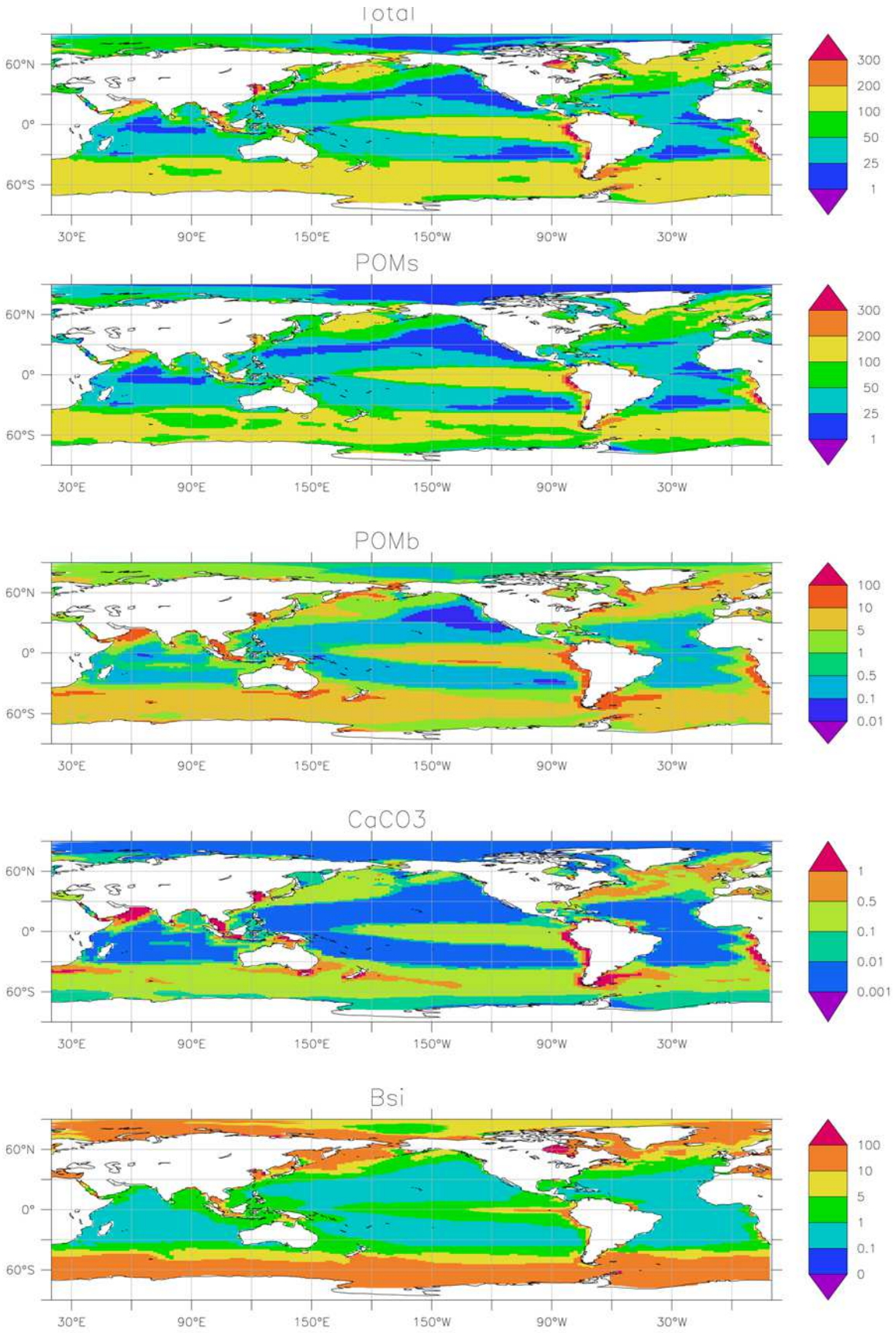
Total
60°N
0°
60°S
30°E
90°E
150°E
150°W
90°W
30°W
300
200
100
50
25
1
POMs
60°N
0°
60°S
30°E
90°E
150°E
150°W
90°W
30°W
300
200
100
50
25
1
POMb
60°N
0°
60°S
30°E
90°E
150°E
150°W
90°W
30°W
100
10
5
1
0.5
0.1
0.01
CaCO3
60°N
0°
60°S
30°E
90°E
150°E
150°W
90°W
30°W
1
0.5
0.1
0.01
0.001
Bsi
60°N
0°
60°S
30°E
90°E
150°E
150°W
90°W
30°W
100
10
5
1
0.1
0

Figure 1

with depth (only one order of magnitude). It is noteworthy that for BSi the Southern Ocean surface maxima extends far deeper in the ocean than for other particle types.

[17] We have made an attempt to evaluate the particle fields simulated by the PISCES model with observations. Although the very limited number of available observations of particles at the global scale makes this comparison difficult, several aspects can be assessed. The total particle concentrations of the model can be compared with the measurements performed along the Western Atlantic GEOSECS section [*Brewer et al.*, 1980] (Figure 3a) and estimates based on nephelometry [*Biscaye and Eittreim*, 1977] (Figure 3b). This comparison reveals that the total particle concentrations are realistically simulated at the surface of the ocean where values agree reasonably well with observations (Figure 3a). At middle water depths (2–3 km), observations indicate lower particle concentrations in the subtropical gyre than at the equator and at high latitudes (Figure 3b). This contrast is also correctly simulated in the model (Figure 2), although concentrations tend to be slightly underestimated at these depths. However, the simulated total particle concentrations in the deep ocean (Figure 2) are too low, relative to observations (Figure 3a), which likely also results from the absence (in our model) of aluminosilicate particles, whose concentration is not negligible [*Spencer*, 1984]. Satellite-derived estimates of POC concentration generated from CZCS particulate backscattering coefficient [*Loisel et al.*, 2002] offers the opportunity to evaluate the spatial structure of POM surface concentrations (Figure 3c). The simulated surface concentrations of POM (mainly small particles in our model) appear realistic compared to the observations for both the spatial structure and the order of magnitude. The only major salient deviation from the observations is found in the Equatorial Pacific Ocean, where the model tends to overestimate the POM concentrations. POM observations at station Papa [*Boyd et al.*, 1999] indicate that the ratio of small versus large particles in surface concentrations (a factor 10) simulated in the model (also a factor 10) is reasonable. However, the vertical structure of simulated POM reveals a serious shortcoming: Although the modeled POM concentration exhibits realistic values at the surface, its vertical gradient between the surface and the bottom of the ocean (3 order of magnitude) is exaggerated (a factor 50 is present in the observations [*Druffel et al.*, 1992; *Sherrell et al.*, 1998]). The POM concentrations are then too low at the bottom of the ocean in our simulations. In our model BSi represents a large contribution to total particle concentrations in the deep Southern Ocean (Figure 2). BSi observations in the Southern Ocean [*Tréguer et al.*, 1990] support the vertical structure simulated by the model, especially in the subsurface where observations indicate a moderate decrease in concentrations with depth. In the PISCES model, $CaCO_3$ has globally lower concentrations than other types of particles (Figures 1 and 2). This appears to be realistic when compared with observations in the Pacific ocean performed by large-volume in situ filtration [*Sherrell et al.*, 1998], which shows $CaCO_3$ concentrations in the water column that are similar to our simulated values.

3.2. Distributions of ^{231}Pa and ^{230}Th

3.2.1. Atlantic Ocean

[18] We first present the results in the Atlantic basin where the number of available observations is the greatest. Figures 4 and 5show the results of the simulations in the Atlantic basin for both dissolved (A_d) and total particulate (small plus large particle, $A_p = A_{POMs} + A_{pb}$) phases for ^{230}Th and ^{231}Pa, respectively. Model results are presented as zonal averages and the observations are superimposed (circle) on the meridional section. In general, the performances of the simulations are similar for ^{231}Pa and ^{230}Th. Exp 1 succeeds in producing a realistic range of values for dissolved activities of the tracers. However, particulate phase concentrations differ drastically from observations, with tracer activities that are two orders of magnitude too low. These results differ from those obtained by *Siddall et al.* [2005] who succeeded in producing more acceptable results with the same coefficient set. This difference arises because in the simulation of *Siddall et al.* [2005] all particle types sink slowly and uniformly (3 m/d), whereas in our model we include a pool of large particles that sink very rapidly. In our first simulation (Exp 1), the more rapidly sinking large particles scavenge the tracer toward the

Figure 1. Particle concentration from the PISCES model at the ocean surface. (a) Total particle concentrations, (b) small particles organic carbon concentrations (POMs), (c) large particles organic carbon concentrations (POMb), (d) calcium carbonate concentrations ($CaCO_3$), and (e) biogenic silica concentrations (BSi). Units are mg/m^3.

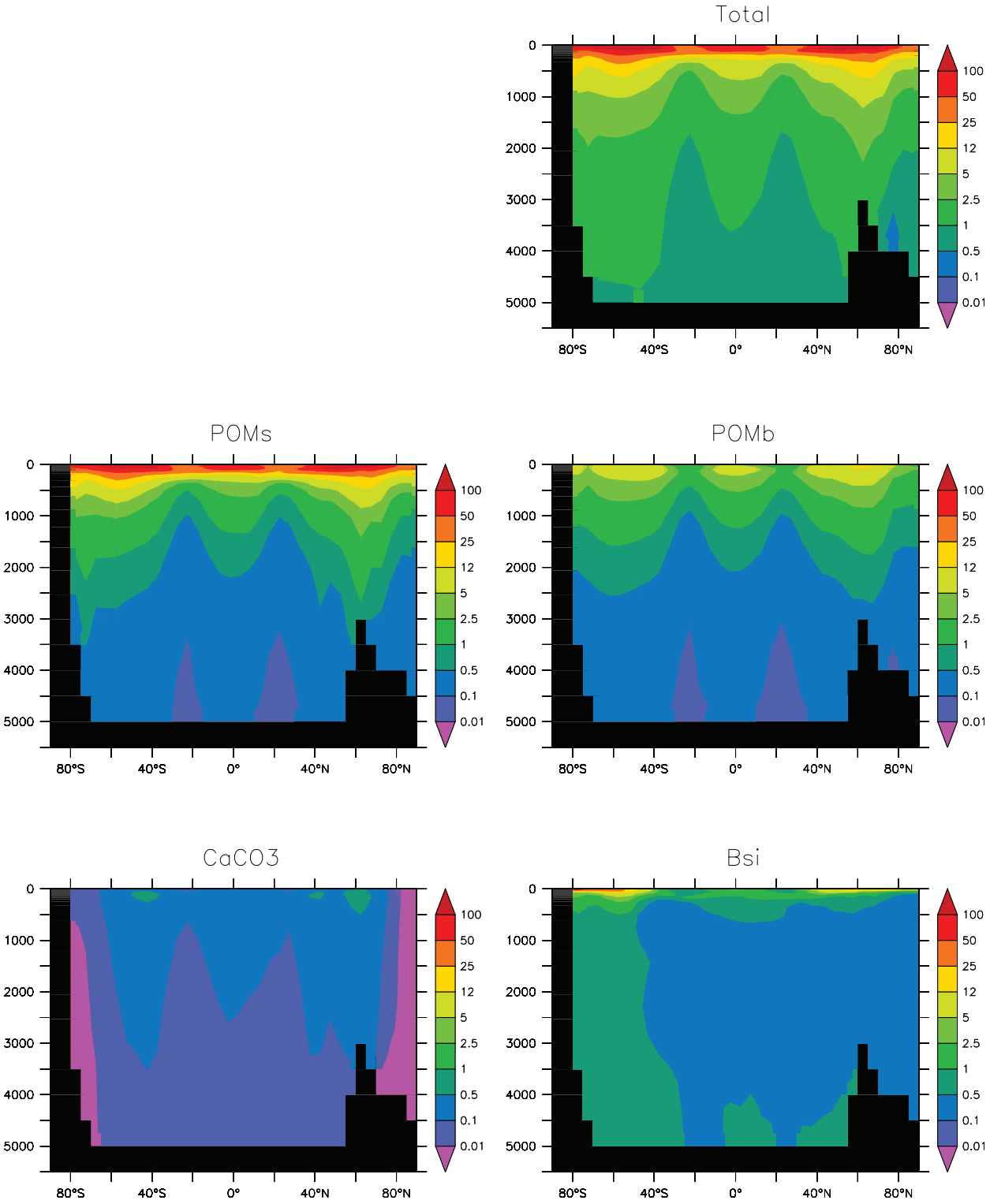

Figure 2. Global zonal averaged of particle concentration. (a) Total particle concentrations, (b) small particles organic carbon concentrations (POMs), (c) large particles organic carbon concentrations (POMb), (d) calcium carbonate concentrations ($CaCO_3$), and (e) biogenic silica concentrations (BSi). Units are mg/m^3.

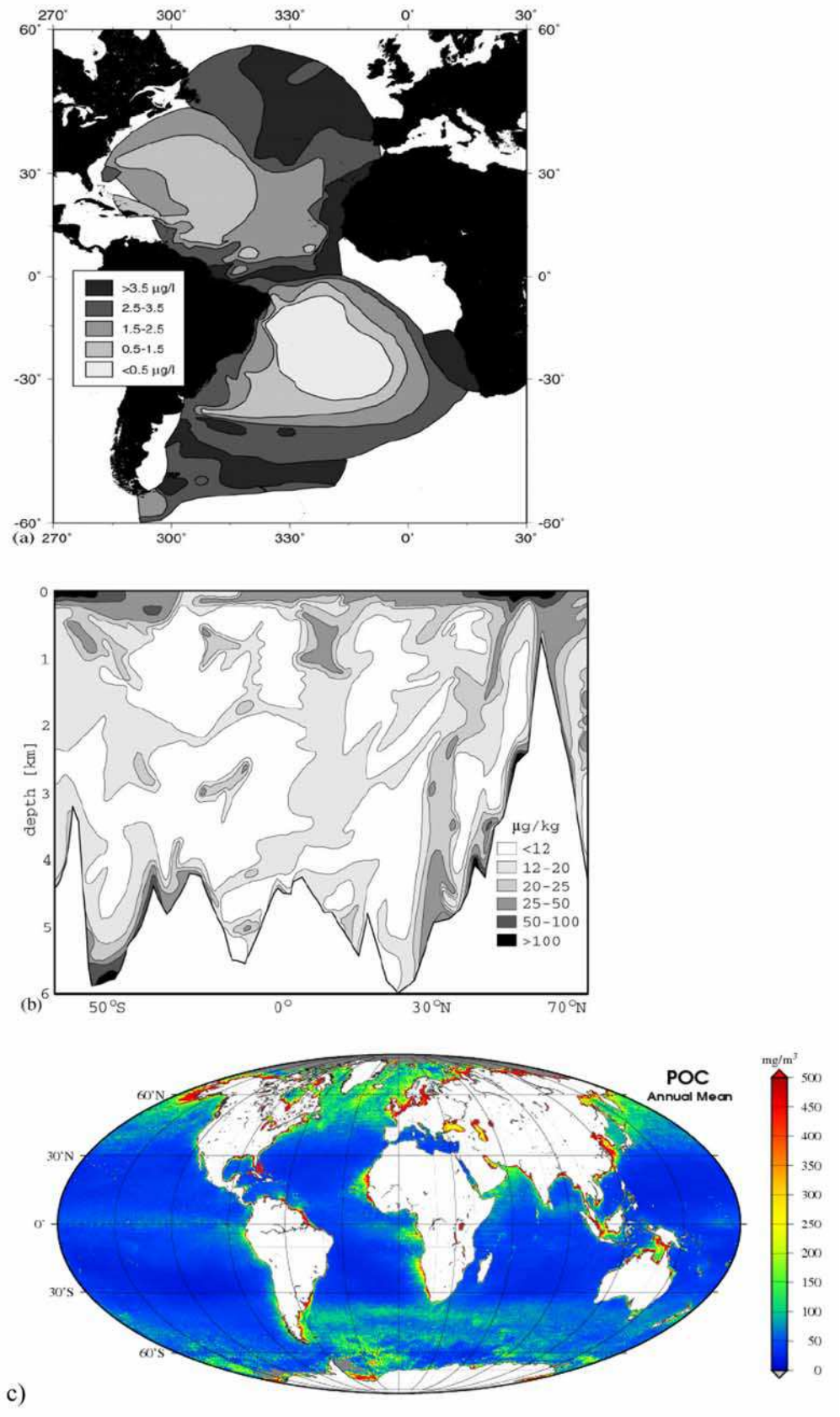
270°
300°
330°
0°
30°
60°
30°
0°
-30°
-60°
>3.5 µg/l
2.5-3.5
1.5-2.5
0.5-1.5
<0.5 µg/l
(a)
depth [km]
0
1
2
3
4
5
6
µg/kg
<12
12-20
20-25
25-50
50-100
>100
(b)
50°S
0°
30°N
70°N
POC
Annual Mean
mg/m³
500
450
400
350
300
250
200
150
100
50
0
60°N
30°N
0°
30°S
60°S
c)

Figure 3

sediment more efficiently such that globally, the water column particulate tracer concentration is too depleted.

[19] These results can be explained in more details by looking at the global budget of ^{231}Pa and ^{230}Th. At equilibrium, the production and radioactive decay of the tracer in the water column must be equal to the sedimentation flux at the bottom of the ocean:

$$\int_{Volume} [\beta - \lambda(A_D + A_P)]dv = \int_{bottom} (-wA_p)ds$$

Neglecting the radioactive decay as regards the production rate, and taking averaged value for the second term, this equation gives the following relationship:

$$\beta z_{oc} = \overline{-wA_P},$$

where

$$\overline{wA_p} = \frac{1}{S}\int wA_p dS$$

where z_{oc} corresponds to an averaged ocean depth (4000 m). Because A_p (^{230}Th) and A_p(^{231}Pa) have typical values of the order of 0.1 dpm m^{-3} and 0.01 dpm m^{-3} at the bottom of the ocean, respectively (Figures 4 and 5), this implies an average sinking velocity of the order of 1000 m/a (or 3 m/d) for both tracers. However, with the two particle classes, the averaged sinking rate in the model (of the order of few 10000 m/a [*Gehlen et al.*, 2006]) may be largely overestimated. This sinking velocity of 1000 m/a matches the sinking velocity of the small particles pool in our model, indicating that the flux to the sediments may have to be controlled by the flux of small particles in order to simulate realistic tracer values. Assuming that the ratio A_p/A_d is of the order of 1/10 in the ocean for both tracers (Figures 4 and 5), and that the POM concentration is of the order of 10^{-8} g/l in the deep ocean (Figure 2), gives a value for Kd of the order of 10^9 for small particles (POM).

[20] Consider then a second simulation wherein the partition coefficient for the small particles is increased to 10^9. This appears larger than Kd values for particulate organic carbon observed in the ocean, which are in general ranking between 10^7 and 10^8. However, these estimates stand for the total concentration of POM. Consequently, as our model that discriminates between small and large particles, we have reduced the value of the Kd for large particle (POMb) (Kd = 10^6) for this second simulation, in order to maintain an average Kd for total particulate organic carbon (POMs + POMb) that is in agreement with the observations. It is consistent with the observations of *Chase et al.* [2004] that show partition coefficients dependent on the intensity of particle flux, with Kd values decreasing when particle flux increases. Moreover, *Scholten et al.* [2005] found a negative correlation between ^{230}Th concentrations and particle fluxes. This feature is also compatible with the constant flux model of *Osmond* [1979] where the tracer concentration is inversely proportional to the particle flux. This configuration is consistent with the hypothesis that most (if not all) ^{230}Th present in trapped particles is in fact carried by small particles aggregated to coarse ones [*Roy-Barman et al.*, 2005]. This is supported by the Kd of Th, which varies by more than an order of magnitude due to the dilution of Th-rich small particles in large aggregates [*Chase et al.*, 2002; *Roy-Barman et al.*, 2005]. Therefore, the Kd of the fine particles must be at least one order of magnitude higher than the Kd of coarse particles for two reasons: First, most ^{230}Th-rich trapped particles are not simply made of aggregated fine particles (they contain foraminifera, fecal pellets, and marine snow which all are coarse particles). Second, in the trapped particles with the lowest ^{230}Th concentrations, the ^{230}Th may be carried by small particles aggregated to the coarse ones [*Roy-Barman et al.*, 2005].

[21] For example, most Kd Th values measured by *Chase et al.* [2002] range from 10^5 to 10^7 g/ml, whereas Kd Th measured directly on suspended particles are in the 2–5 $\times$ 10^7 g/ml range [*Bacon and Anderson*, 1982; *Bacon et al.*, 1989; *Trimble et al.*, 2004]. However, a 1000 fold difference in the Kd for fine versus coarse particles appears to be overestimated compared to the prediction from the observations. For instance, a factor 3 or 4 is observed on the ^{231}Pa and ^{230}Th concentrations between the small particles collected by in situ filtration and large particles collected by sediment traps in the equatorial Atlantic [*Anderson et al.*,

Figure 3. (a) Particle concentrations measured along the W. Atlantic GEOSECS section [*Brewer et al.*, 1976] in units of μg/kg. (b) Particle concentrations at middepth in the water column (2–3 km) based on nephelometry [*Biscaye and Eittreim*, 1977]. (c) Satellite-derived estimation of POM generated from CZCS particulate backscattering coefficient (H. Loisel et al., personal communication, 2002).

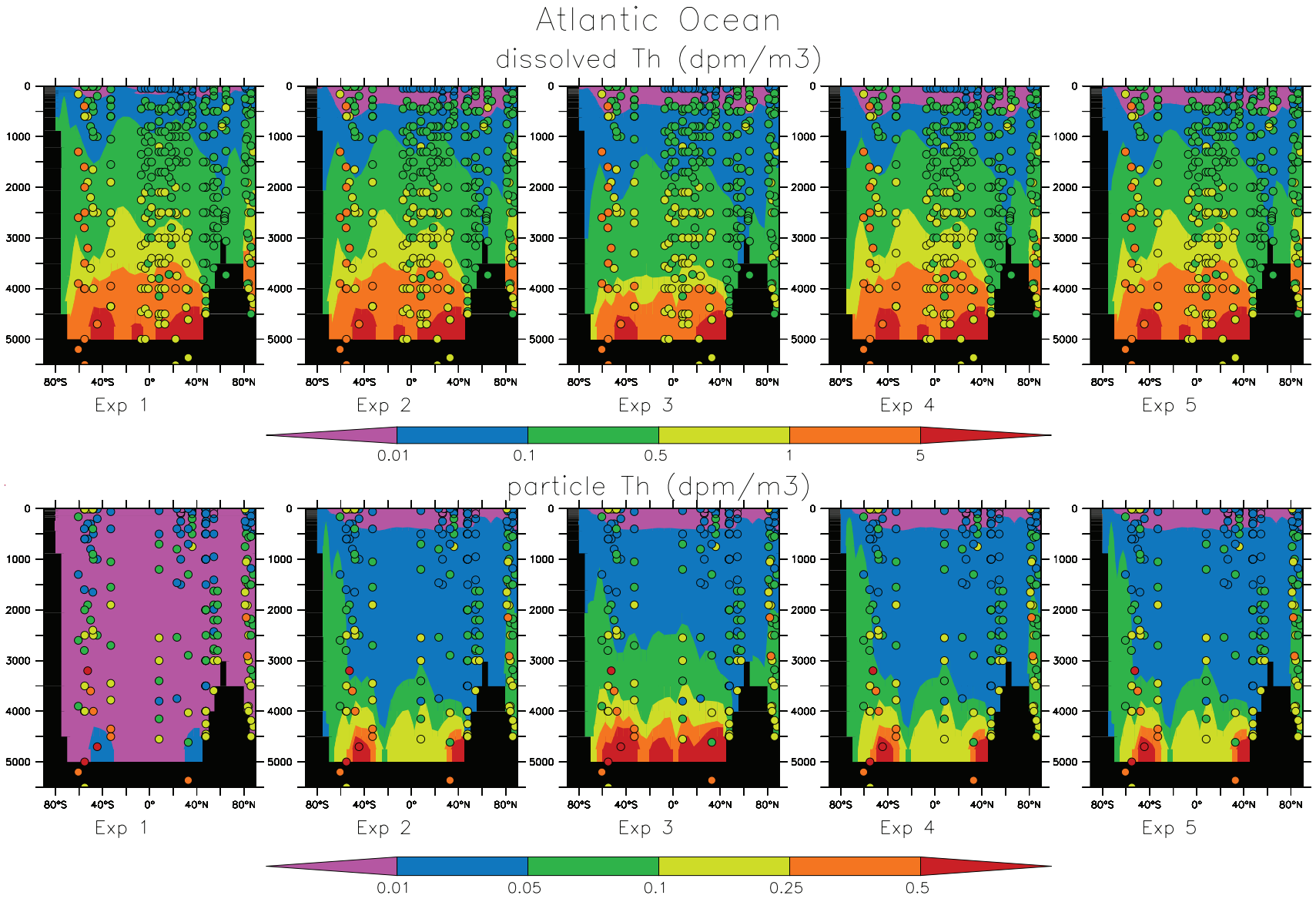

Figure 4. Simulated zonal dissolved and particulate distributions of ^{230}Th in the Atlantic Ocean. Observations are represented by the circles. Units are dpm/m^3.

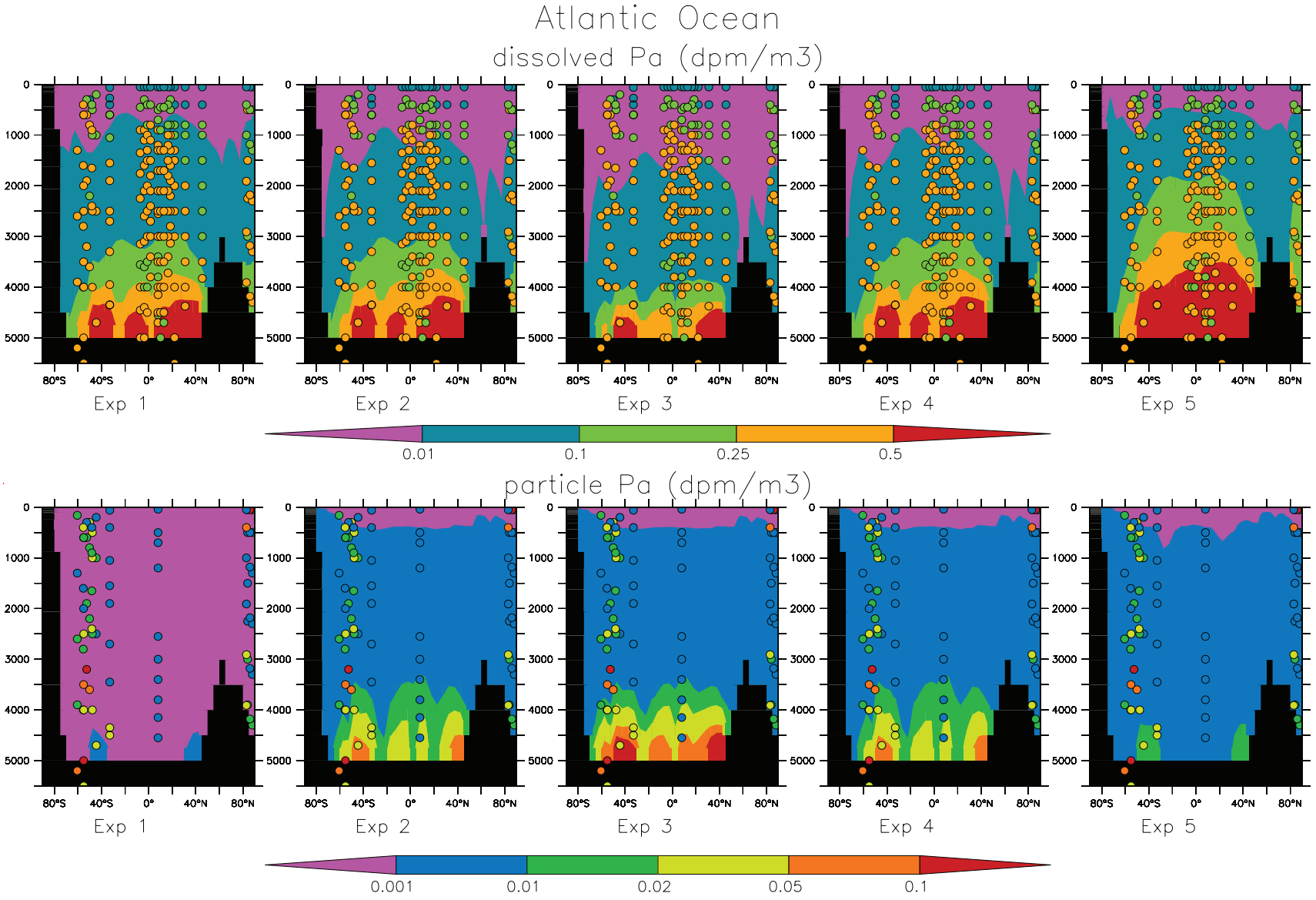

Figure 5. Simulated zonal dissolved and particulate distributions of ^{231}Pa in the Atlantic Ocean. Observations are represented by the circles. Units are dpm/m^3.

1983], and a factor 50 is estimated for the variation of the Kd as a function of the particle flux [*Chase et al.*, 2002]. But the very low concentrations of small particles simulated at the bottom of the ocean in the PISCES model drives the use of such a large coefficient for the small particles. Such large changes in the values of the partition coefficients result in noticeable improvements during Exp 2. The activities in the dissolved phase remain realistic, but for both ^{231}Pa and ^{230}Th, the activities simulated in the particulate phase increased to values more compatible with the observations (Figure 4).

[22] However, a considerable shortcoming still remains in the modeled vertical profiles. In general, the simulated vertical structure exhibits a salient maximum at the bottom of the ocean, which compensates for a relative depletion of the tracer at shallower depths in the water column, compared to the more uniform vertical distribution seen in the observations. This shortcoming also existed in the simulations performed by *Siddall et al.* [2005], but not in the work of *Henderson et al.* [1999] who used a parameterization of the partition coefficient as a function of the mass of particles. This unrealistic accumulation of tracers near the bottom of the ocean may give the impression that scavenging is too rapid in the water column and too low at the bottom. We have investigated this aspect in more detail via sensitivity tests performed on the partition coefficients of the rapid sinking particles (not shown). Changing the values of the partition coefficients on the rapidly sinking particles in our model does not improve the shape of the vertical profiles as this shape is mainly controlled by the flux of small particles. Because the decrease in the concentration of small particles with depth is overestimated in our model (see section 3.1), the tracers tend to accumulate in the dissolved phase at the bottom of the ocean. Compensating for this effect, we therefore tested the parameterization used by *Henderson et al.* [1999], where Kd vary with the logarithm of particle concentration [*Honeyman et al.*, 1988] and implemented this for the small particles in our model (Table 1, Exp 3). Because small particles have a uniform sinking velocity in the model, this parameterization can also be interpreted as though the partition coefficient varies as a function of particle flux (as suggested by *Chase et al.* [2004]). Considering the range in the concentration of small particles simulated in our model (Figure 2), this parameterization can generate variations of Kd of two orders of magnitude in the water column. As the concentration of POM decreases with depth (Figure 2), this parameterization generates lower Kd with more realistic values of the order of 10^8 near the surface, and higher Kd that reduces the dissolved tracer concentration at the bottom of the ocean. Therefore, it generates more uniform profiles in the water column in agreement with the observations (Figures 3 and 4). On the other hand, the activities of the tracer are increased in the particulate phase, which is evidently an improvement for ^{230}Th, but is less convincing for ^{231}Pa due to the disparity in the observations. The parameterization also tends to generate a global reduction in the total concentration of the tracers in the water column that is not satisfactory. This feature could be improved by changing the reference value of Kd; however, the goal of this paper is not to provide a calibration of the partition coefficient but to show the impact of different Kd values.

[23] We now show results from two other sensitivity tests (Exp 4 and Exp 5), which were performed to examine a particular aspect of the tracer distribution. They accentuate the contrast in the affinities of ^{231}Pa and ^{230}Th for particles (Table 1), which will be particularly relevant in considering the ^{231}Pa/^{230}Th ratio in the flux to the sediment. In the previous simulations, the largest discrepancies between the model and the observations for dissolved ^{230}Th were found in the Southern Ocean (Figure 4), where simulated ^{230}Th activities were remarkably low. In our model this sector is characterized by high concentrations of BSi that extend deep in the ocean (Figure 2). In Exp 4 we attempted to improve the simulated ^{230}Th distribution by reducing its partition coefficient for BSi by a factor of 10 (see Table 1). The realism of this configuration is supported by the results of *Chase et al.* [2002], showing that the relative affinity of ^{230}Th for BSi decreases compared to ^{231}Pa when the percentage of opal is increasing (see Figure 2 in the work of *Chase et al.* [2002]). This configuration provides a noticeable improvement in the Southern Ocean where the simulated dissolved activity of ^{230}Th is elevated, although this activity remains too low compared to the observation. Thus, decreasing the affinity of ^{230}Th for BSi would lead to an improvement of the simulation, but it would also generate a very low partition coefficient, relative to observational estimates.

[24] In comparison with ^{230}Th, the dissolved ^{231}Pa appears more depleted globally relative to the observations (Figures 4 and 5). This feature suggests that the partition coefficients for ^{231}Pa are too

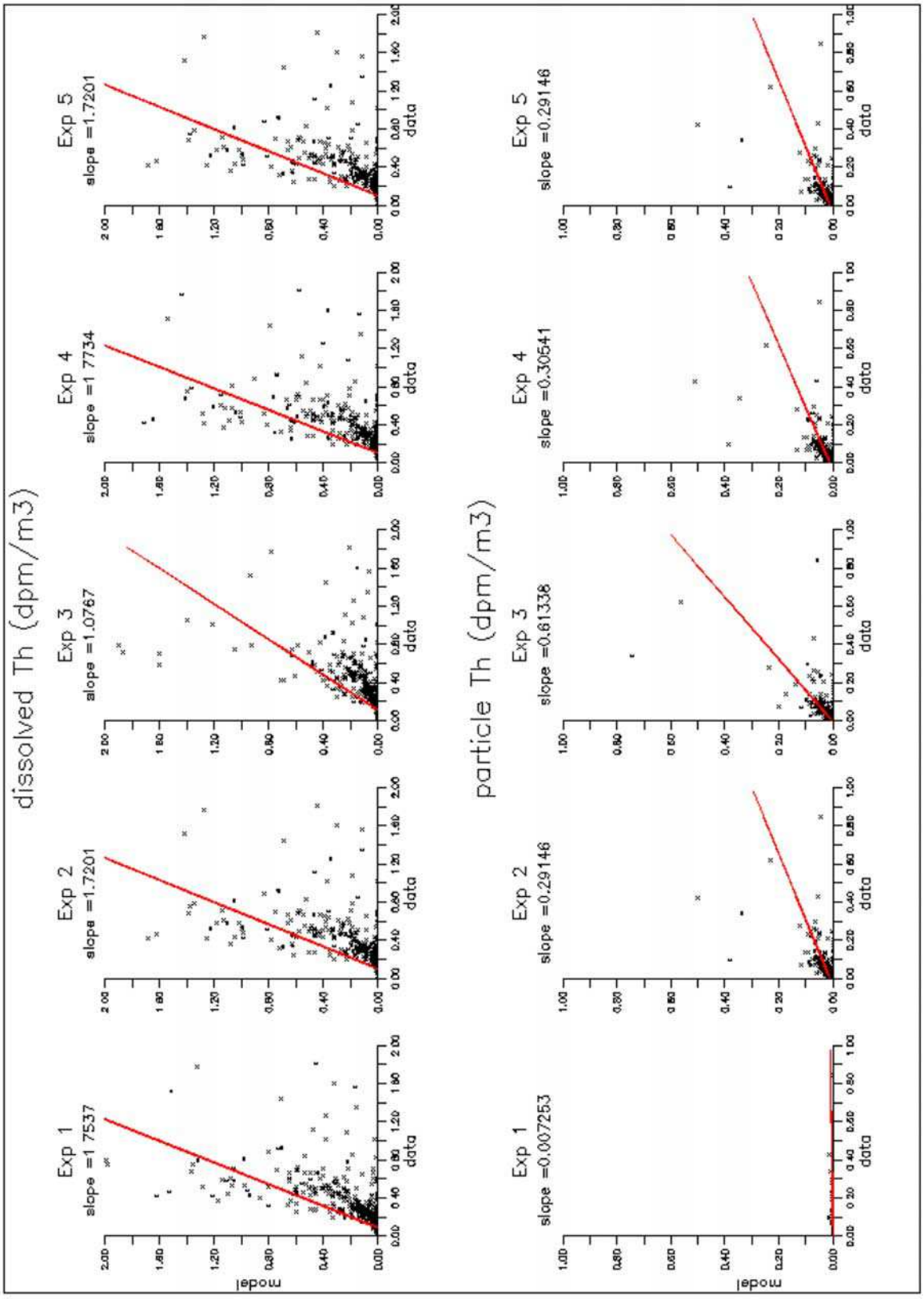

Figure 6. Model/data linear regression of dissolved and particulate ^{230}Th in the Atlantic Ocean. Units are dpm/m^3.

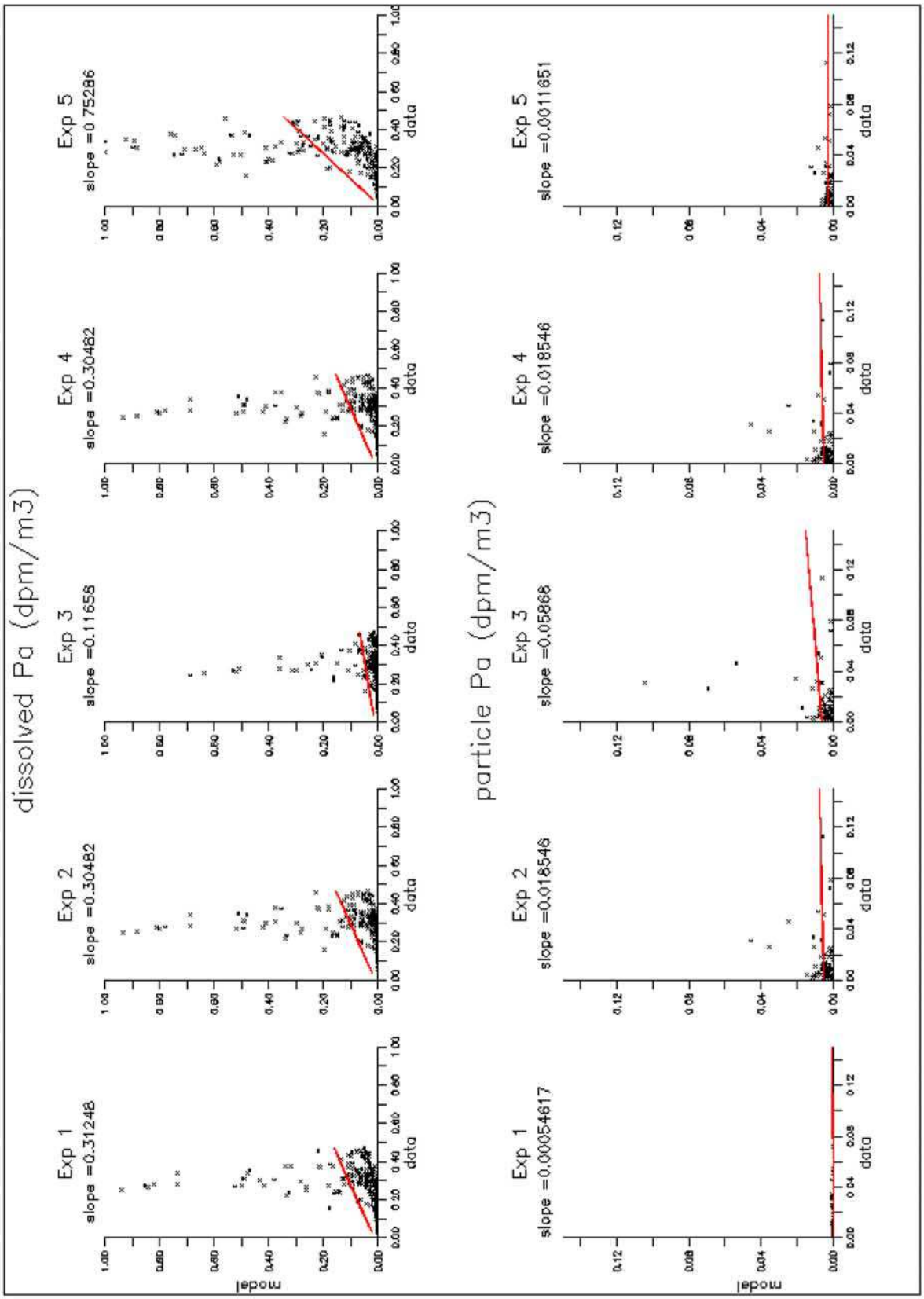

Figure 7. Model/data linear regression of dissolved and particulate ^{231}Pa in the Atlantic Ocean. Units are dpm/m^3.

large. In Exp 5, we reduce the partition coefficient of ^{231}Pa for small particles (POM) by a factor 5 (Table 1). This approach is supported by many observationally based estimates, which indicate a lesser partition coefficient for ^{231}Pa than for ^{230}Th for POM [*Luo and Ku*, 1999; *Chase et al.*, 2002; *Chase and Anderson*, 2004; *Luo and Ku*, 2004]. The reduction in the partition coefficient on small particles for ^{231}Pa greatly improves the simulated distribution in dissolved phase for the Atlantic Ocean (Figure 5). However, the results for the particulate phase of ^{231}Pa appear less clear. Model results are improved in the tropical Atlantic Ocean, when compared to the unique profile available in this region, but in the south the disparity present in the observations does not allow us to discern this unambiguously.

[25] In order to provide a more quantitative evaluation of the simulations, we have performed linear regressions between model and observations for ^{231}Pa and ^{230}Th (Figure 6 and 7). These plots show a large scatter between model and observations for all experiments. The values of the slope of the linear regressions represent an indicator of the ability of the model to simulate the tracer distribution. The plots particularly illustrate the improvement for the modeled ^{230}Th distribution when the partition coefficient of POMs is parameterized as a function of the mass of particles: the slope of the linear regression changes from 1.72 to 1.08 for the dissolved phase and from 0.29 to 0.61 for the particulate phase, between Exp 2 and Exp 3 (Figure 6). However, this diagnostic also reveals worse performances for ^{231}Pa simulations, in which the slopes of the linear regressions remain too low (Figure 7). This is especially the case for the particulate phase of ^{231}Pa, where the number of observations is small, and the model fails to reproduce the high values observed in the Southern Ocean (Figure 5). The improvement between Exp 2 and Exp 3 in the simulation of ^{231}Pa is less evident than for ^{230}Th, because the value of the slope increases for the particulate phase, but declines for the dissolved phase. However, reducing the value of the partition coefficient for POMs greatly improves the correspondence between the model and observations for the dissolved phase, with a slope that increases from 0.30 in exp 2 to 0.75 in Exp 5. However, our systematic underestimation of ^{231}Pa concentration in the particulate phase is exacerbated.

3.2.2. Pacific and Indian Oceans

[26] In comparison with the Atlantic Ocean, there is, at present, considerably less ^{231}Pa and ^{230}Th data available in the Pacific and Indian Oceans for comparison with our simulations. For this reason, it is not always possible to assess both the simulated dissolved and particulate phases of the tracers as performed for the Atlantic Ocean in section 3.2.1. In the Pacific Ocean, ^{230}Th observations are available for the dissolved and particulate phases (Figure 8), but due to the limited number of ^{231}Pa observations for particles, the simulations are compared with measurements of dissolved and total ^{231}Pa, for which observations are more numerous (Figure 9). In the Indian Ocean, the even more limited number of observations forces us to consider the total concentrations of the two tracers (Figure 10).

[27] The evaluation of the different simulations in the Pacific and Indian Oceans results in similar conclusions as for the Atlantic Ocean. For instance, in the Pacific Ocean, we recover similar performances of the different simulations in producing a realistic range of values for both the dissolved and particulate phases of ^{230}Th (Figure 8). In particular, indentical partition coefficients for the small and large POM (Exp 1), results in unrealistically low tracer activities in the particulate phase, while for the experiments with higher values of the partition coefficients for small particles (Exp 2, 3, 4, and 5), the results become more realistic (Figure 8). Moreover, the general trends observed in the sensitivity tests in the Atlantic are also found in the Pacific and Indian Oceans. More specifically, reducing the partition coefficients of POM for ^{231}Pa (Exp 5) produces higher total activities, in better agreement with the observations, and reducing the partition coefficients of BSi for ^{230}Th (Exp 4) improves the results in every sector of the Southern Ocean. Due to the different oceanic residence times of ^{231}Pa and ^{230}Th, an interesting contrast between the two tracers is observed in the Indian Ocean. ^{230}Th measurements show an increase in concentration with depth, although ^{231}Pa measurements exhibit a maxima at around 2500 m depth. This represents a water mass originating from the South Atlantic Ocean, having a distinct signature relative to the water masses originating from the Antarctic Circumpolar Current (ACC) that are more depleted due to the efficient scavenging by BSi [*Thomas et al.*, 2006]. However, our model fails to correctly reproduce this observed feature in the ^{231}Pa profiles. This is because the simulations performed with the coarse horizontal resolution (2° × 2°) results in an overestimation of the Indian Ocean ventilation from the ACC [*Lachkar et al.*, 2007], which prevents us reproducing the observed South Atlantic ^{231}Pa concentrations.

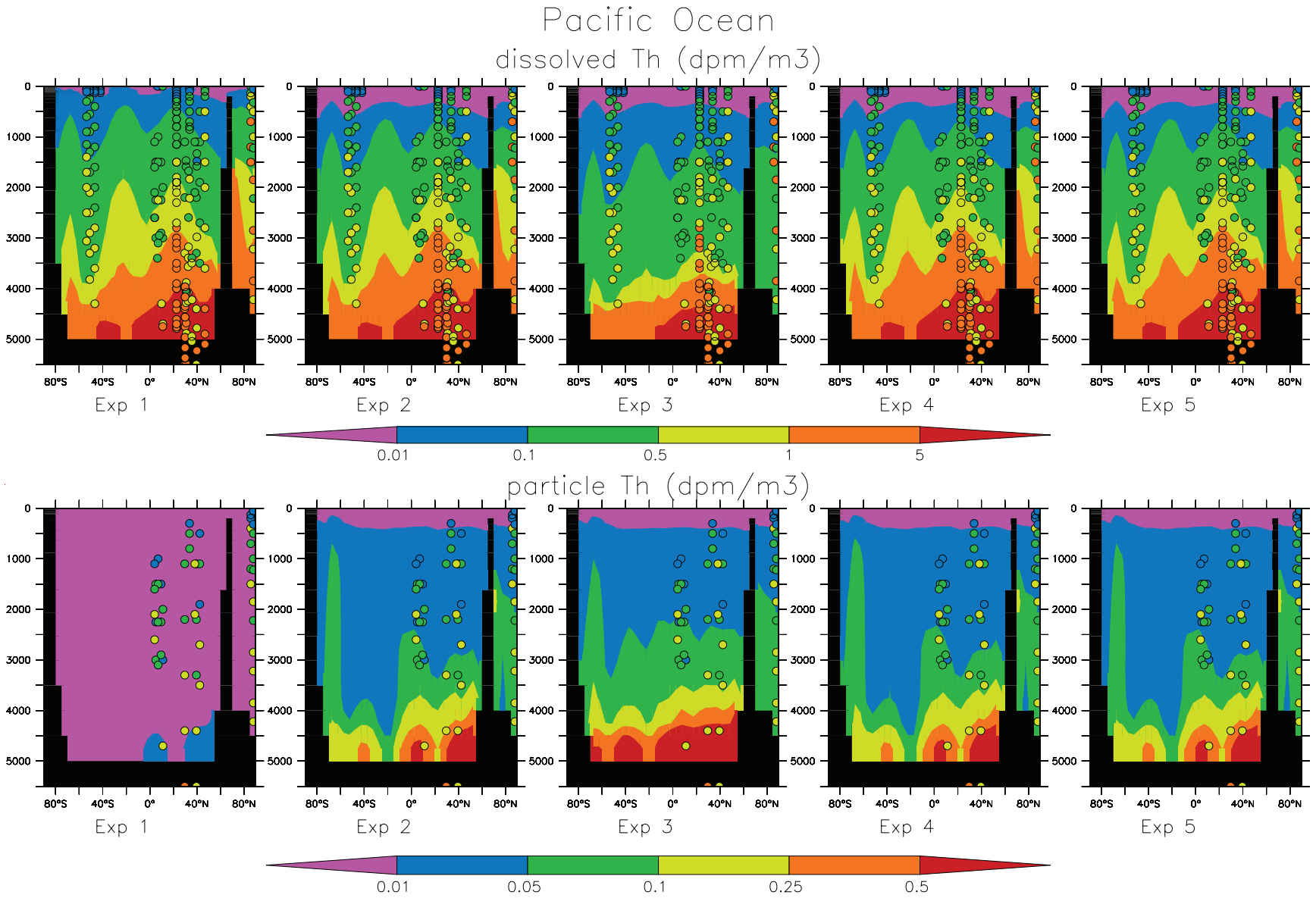

Figure 8. Simulated zonal dissolved and particulate distributions of ^{230}Th in the Pacific Ocean. Observations are represented by the circles. Units are dpm/m^3.

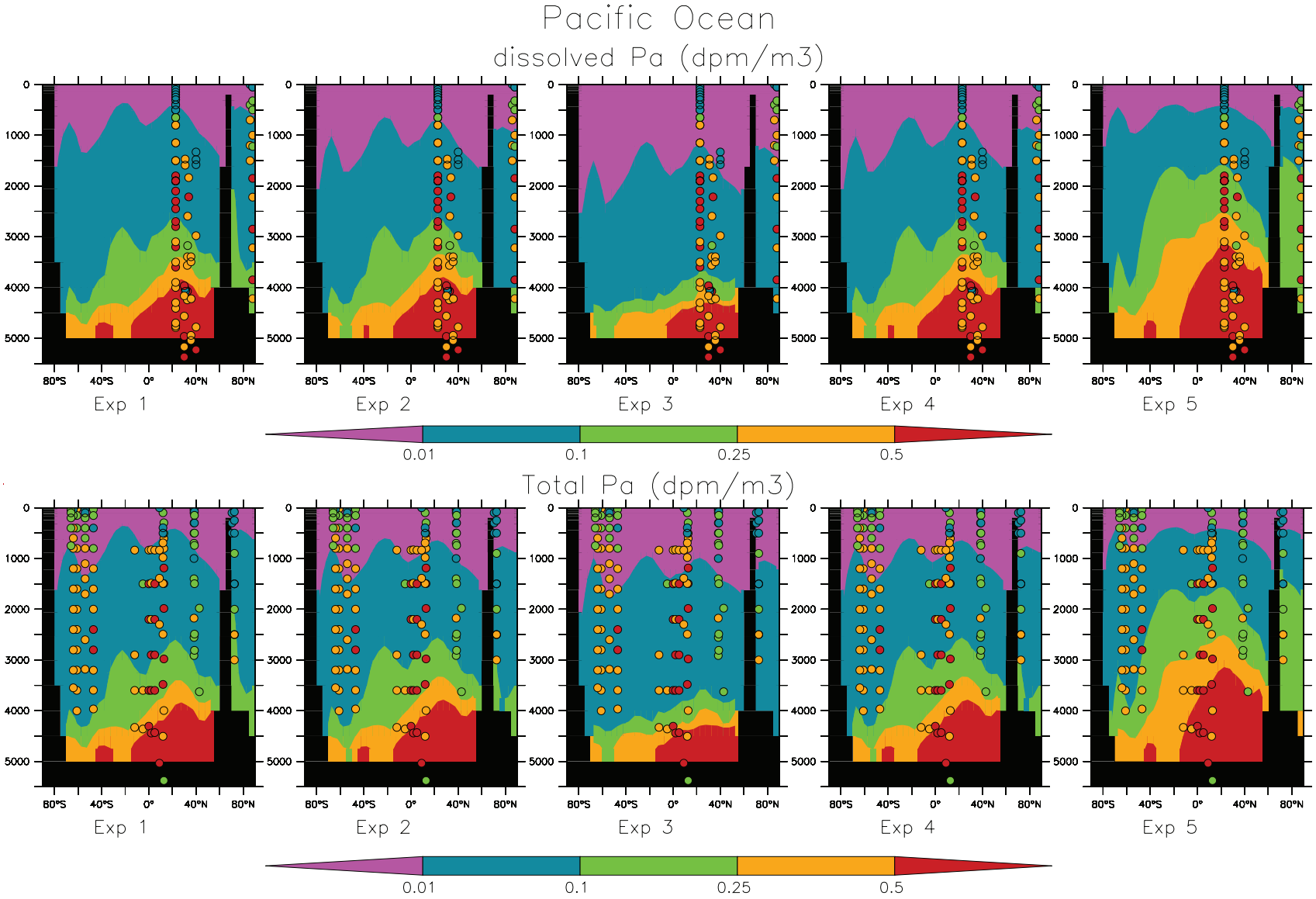

Figure 9. Simulated zonal dissolved and total distributions of ^{231}Pa in the Pacific Ocean. Observations are represented by the circles. Units are dpm/m^3.

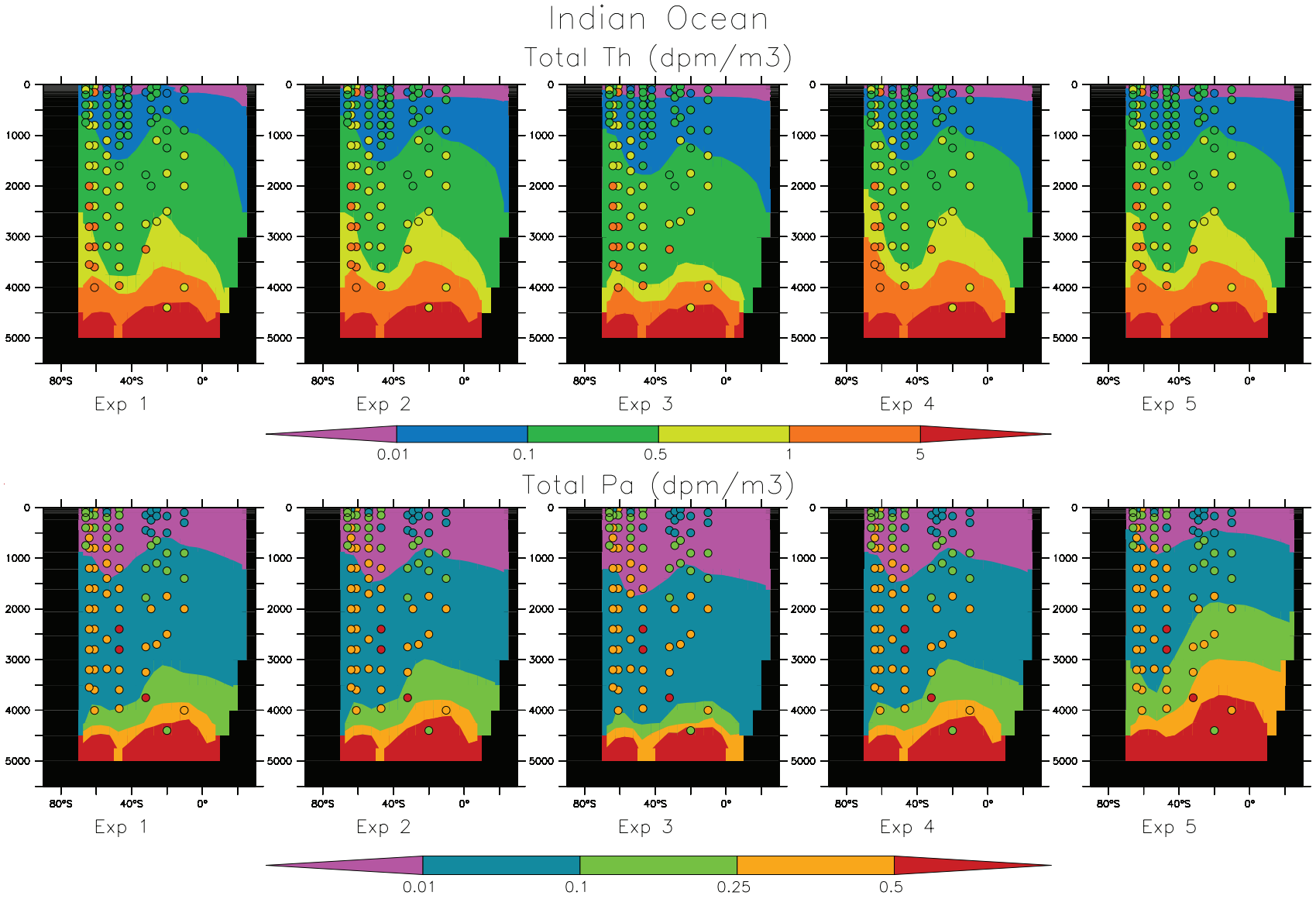

Figure 10. Simulated zonal distributions of total ^{230}Th and ^{231}Pa in the Indian Ocean. Observations are represented by the circles. Units are dpm/m^3.

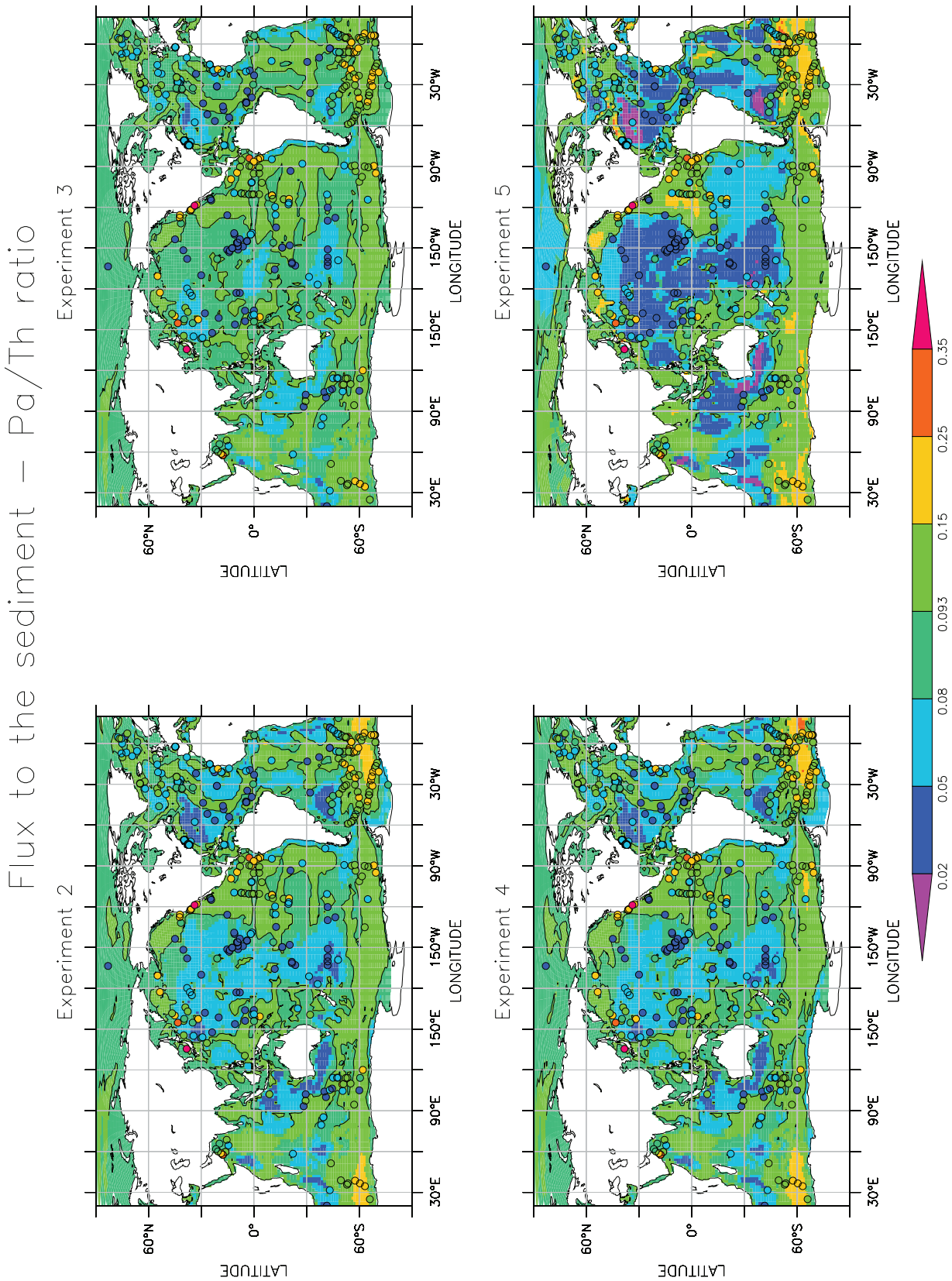

Figure 11. Simulated ^{231}Pa/^{230}Th in the flux to the sediment. Observations are represented by the circles. Units are dpm/m^3.

3.3. ^{231}Pa/^{230}Th Ratio in the Flux to the Sediment

[28] We now assess the ^{231}Pa/^{230}Th ratio in the flux to the sediments, which is of special interest for paleoclimatologic studies. Figure 11 shows the simulated distribution of the ^{231}Pa/^{230}Th ratio in the total flux of particles to the sediment (small plus large particles) for the four experiments that provide the most realistic results in the water column (Exp 2, 3, 4, and 5). Observations (circles) are superimposed onto model results. Observations indicate a ^{231}Pa/^{230}Th ratio above the production rates (0.093) in the eastern equatorial Pacific Ocean where productivity is high (Figure 1), and in the Southern Ocean where removal of ^{231}Pa is efficient (due to the large flux of BSi in this region; Figures 1 and 2). Coastal regions are also generally associated with a ratio greater than the production rate. It reflects the concept of "boundary scavenging" [*Anderson et al.*, 1983], with higher ^{231}Pa/^{230}Th ratios near continental margins where the particule flux is high and lower ratios in the open ocean where the particle flux is lower.

[29] Exp 2 produces a distribution of the ^{231}Pa/^{230}Th sediment flux ratio that differs in some aspects from the observations. The higher ^{231}Pa/^{230}Th ratio in the Southern Ocean and eastern equatorial Pacific Ocean are qualitatively represented, but the simulation tends to systematically overestimate the values in the regions of low productivity, where the observed ratio is below the production rate. This characteristic appears to arise because the flux is globally controlled by small particles (see section 3.2.1), with identical values of the partition coefficient for the two tracers. This leads to a similar residence time for the two tracers in the water column that does not permit the particle flux to generate a realistic contrast between the two tracers in the sediment flux. This feature is exacerbated in Exp 3, where the parameterization of the partition coefficient as a function of the mass of small particles acts to increase the relative contribution of small particles at the bottom of the ocean and subsequently in the sediment flux. We also observe higher ratios near regions where the water depth is relatively shallow, such as the Mid-Atlantic Ridge (MAR). This feature appears in our simulations because the low ^{231}Pa/^{230}Th ratios are mainly generated by the difference in affinity for the two tracers in the large particle pool (Kd_{Bsi} is larger for ^{231}Pa than ^{230}Th, and Kd_{caco3} is larger for ^{230}Th than for ^{231}Pa; see Table 1). The imprint of the pool of large particles on the ^{231}Pa/^{230}Th ratio becomes more noticeable in the particle flux at depth because their settling rate increases (see section 2.2). The performance changes only moderately in Exp 4, where the contrast between the two tracers is enhanced in the pool of large particles for Bsi. The main difference is higher values of the ^{231}Pa/^{230}Th ratio in the Southern Ocean, but the general shortcomings persist as the flux is controlled by the small particles. Nevertheless, a considerable improvement is obtained in Exp 5 where a fractionation is introduced for the small particles of particulate organic carbon (POMs). This simulation provides a more realistic representation of ^{231}Pa/^{230}Th ratio, especially for the values below the production ratio. We also observe a general extension of the regions with a ratio larger than the production ratio at the high latitudes in this simulation.

4. Conclusions

[30] We have simulated ^{231}Pa and ^{230}Th distributions with a general circulation model (NEMO) that is coupled to a biogeochemical model (PISCES). The major discrepancies in our simulation are due to the performance of the PISCES model. The PISCES model was developed for carbon and ecosystem studies and is used here for the first time to simulate the distribution of nonconservative geochemical tracers. Because the model was not originally designed for this objective, we have found significant difficulties (particle concentrations, tracers' vertical profiles, partition coefficient values ...). This analysis is an opportunity to provide an additional evaluation of the particle fields simulated by the PISCES model and to consider possible improvements in order that this model better simulates trace elements distributions. The model considers two categories of particles with different sinking velocities, namely, small particles (POMs) that sink slowly (3 m/d) and large particles (POMb, $CaCO_3$, BSi) that sink more rapidly (50–200 m/d) and simulated carbon fluxes compare reasonably well with sediment trap observations [*Gehlen et al.*, 2006]. A comparison with the few existing observations of particle concentration revealed that PISCES simulates globally realistic particle concentrations at the surface of the ocean but largely underestimates in the deep ocean. Moreover, the ^{231}Pa and ^{230}Th simulations are more realistic when tracer fluxes are controlled by the pool of small particles. The very low concentration of small particles simulated in the deep ocean with the PISCES model have driven us

to employ exaggerated large partition coefficients for fine particles in order to generate realistic tracer distributions. Some improvements in the PISCES model, which cannot be tested in this preliminary analysis, are necessary in order to improve trace element simulations. To increase the concentration of small particles in the deep ocean, several suggestions can be considered: modifications of both the dissolution/remineralization rates and sinking speeds should permit changing particle concentrations without modifying fluxes; introducing BSi, $CaCO_3$, aluminosilicates particles, and possibly Mn oxides into the small particle pool or an additional pool of refractory particles that sink without remineralizing would also tend to increase the particle concentrations in the deep ocean. These improvements will be useful not only for the Pa-Th modeling, but will also improve simulation of other particle reactive metals (Nd, Fe) already present in the model. More generally, it is also possible to improve the parameterization of other important processes, such as ballasting.

[31] The second objective of this study was to use the numerical model to improve our knowledge regarding the processes that control the distributions of trace elements. Previous studies, with simple box models, have already demonstrated the importance of using scavenging models that include two particle classes (small and large) [*Clegg and Witfield*, 1991; *Thomas et al.*, 2006]. We have included such details in a more complex general circulation model via a rather rudimentary representation (''reversible scavenging model''). Some inconsistencies in the particle fields forced us to use unrealistically high values for the small particle partition coefficient in order to obtain more realistic tracer distributions. However, some large deviations between the observations and our simulations remain. It therefore appears difficult to derive some definitive conclusions upon the behavior the trace elements in the ocean from these simulations. Nevertheless, some important features that found support with observations can be mentioned for further assessment in future studies. In particular, distinct partition coefficients for small and large particles are necessary to obtain realistic results. This aspect is supported by observations that reveal a negative correlation between concentration and particle flux [*Chase and Anderson*, 2004; *Scholten et al.*, 2005]. In addition, model results are improved when a reduced partition coefficient for POM is applied for ^{231}Pa, relative to ^{230}Th. The improvement is not only noticeable in the water column, where total ^{231}Pa concentrations are increased, but also for the sediment flux, where it appears to generate the contrast in ^{231}Pa/^{230}Th ratios between the region of low and high productivity that is observed at the global scale. This difference in the affinity for ^{231}Pa and ^{230}Th of POM is supported by the observations [*Chase et al.*, 2002; *Luo and Ku*, 2004; *Roy-Barman et al.*, 2005]. Such a difference was considered in the model of *Marchal et al.* [2000] but ignored in the simulation of *Siddall et al.* [2005], where it had no obvious consequence in their simulation of the ^{231}Pa/^{230}Th ratio in the sediment because all particle types had the same sinking velocity. However, including BSi and $CaCO_3$ in the small particle pool represents another means by which to better represent the fractionation between the two trace elements. This development would also help to better simulate the ^{231}Pa/^{230}Th ratio at middle water depths, where the signal simulated in the model is mainly controlled by the flux of small particles.

[32] This preliminary study has highlighted some difficulties encountered when using two particle size classes to model Pa/Th, even though this remains a simplification when considering the complexity present in the observations [*Kriest and Evans*, 1999]. We have proposed some future model developments that would likely improve future simulations. This study also represents a basis for introducing even more refinement in the model, such as considering particle sinking velocities calculated as a function of particle size and particle number [*Kriest and Evans*, 1999; *Gehlen et al.*, 2006], which would represent a better basis upon which to represent the scavenging of tracers.

Appendix A: Dynamics of Particles in the PISCES Model

[33] The PISCES model has two particle classes. Small particles consist of particulate organic carbon (POMs) sinking with a constant velocity of 3 m/d. The large particles pool contains particulate organic carbon (POMb), calcite ($CaC0_3$), and biogenic silica (BSi) with a settling velocity (w_b) that increases with depth, as shown by *Berelson* [2001].

$$w_b = w_{\min} + (w_{\max} - w_{\min}) \max\left(0, \frac{z - z_m}{2000}\right)$$

where w_{min} is the minimum sinking speed, 50 m/d; w_{max} is the maximum sinking, 200 m/d; and z_m is the mixed layer depth.

[34] The two POM size classes POM_s (small) and POM_b (big) are fueled by mortality of nanophytoplankton and diatoms, fecal pellet production, grazing, and aggregation between DOC, POMs, and POMb. The aggregation term between the two classes of POM writes:

$$\Phi_{agg}(POM_s \rightarrow POM_b) = \Phi^1 shPOM_s^2 + \Phi^2 shPOM_b.POM_s + \Phi^3 POM_s^2 + \Phi^4 POM_s.POM_b$$

The shear rate (sh) is set to 1 s^{-1} in the mixed layer and 0.01 s^{-1} below. The coefficients φ^1, φ^2 for turbulence coagulation and φ^3, φ^4 for differential settling are computing by integrating the standard rectilinear kernels for collisions [*Kriest*, 2002]. The degradation rate of POM_b and POM_s, in POM_s and DOM, respectively, λ_{POM}, depends on temperature with a Q_{10} of about 1.9.

[35] Calcite is fueled by mortality of calcifying nanophytoplankton and by grazing by both types of zooplankton on calcifying nanophytoplankton. The dissolution rate (λ_{CaCO3}) is defined as follows:

$$\Delta CO_3 = \max\left(0, CO_{3SAT}^{2-} - CO_3^{2-}\right)$$

$$\lambda_{CaCO3} = \lambda \frac{\Delta CO_3}{K_{CaCO_3} + \Delta CO_3}$$

This means that no dissolution is allowed in case of oversaturation. On the other hand dissolution increases with the undersaturation.

[36] The biogenic silica is fueled by mortality of diatoms and grazing by both types of zooplankton on diatoms. Its dissolution rate (λ_{BSi}) depends on in situ temperature and on saturation following the parameterization proposed by *Ridgwell et al.* [2002]. For more details on the equation, see http://www.lodyc.jussieu.fr/~aumont/pisces_ description.html.

Acknowledgments

[37] We acknowledge R. Francois for providing unpublished water column data, H. Loisel and D. Dessailly for providing the map of POM generated from CZCS particulate backscattering coefficient, and G. Henderson for providing on line databases of ^{231}Pa/^{230}Th in the water column and in the sediments and for the useful discussions for improving our manuscript. The constructive review of an anonymous reviewer has also improved the manuscript.

References

Anderson, R. F., M. P. Bacon, and P. G. Brewer (1983), Removal of ^{230}Th and ^{231}Pa from the open ocean, *Earth Planet. Sci. Lett.*, *62*, 7–23, doi:10.1016/0012-821X(83)90067-5.

Arsouze, T., J. Dutay, F. Lacan, and C. Jeandel (2007), Modeling the neodymium isotopic composition with a global ocean general circulation model, *Chem. Geol.*, *239*, 165–177, doi:10.1016/j.chemgeo.2006.12.006.

Aumont, O., and L. Bopp (2006), Globalizing results from ocean in situ iron fertilization studies, *Global Biogeochem. Cycles*, *20*, GB2017, doi:10.1029/2005GB002591.

Bacon, M., and R. Anderson (1982), Distribution of thorium isotopes between dissolved and particulate forms in the deep sea, *J. Geophys. Res.*, *87*, 2045–2056, doi:10.1029/JC087iC03p02045.

Bacon, M. P., C.-A. Huh, and R. M. Moore (1989), Vertical profile of some natural radionuclides over the Alpha Ridge, Arctic Ocean, *Earth Planet. Sci. Lett.*, *95*, 15–22.

Beckmann, A., and R. Döscher (1997), A method for improved representation of dense water spreading over topography in geopotential-coordinate models, *J. Phys. Oceanogr.*, *27*, 581–591, doi:10.1175/1520-0485(1997)027<0581:AMFIRO>2.0.CO;2.

Berelson, W. (2001), Particle settling rates increase with depth in the ocean, *Deep Sea Res., Part II*, *49*, 237–251, doi:10.1016/S0967-0645(01)00102-3.

Biscaye, P. E., and S. L. Eittreim (1977), Suspended particulate loads and transports in the nepheloid layer of the abyssal Atlantic ocean, *Mar. Geol.*, *23*, 155–172, doi:10.1016/0025-3227(77)90087-1.

Blanke, B., and P. Delecluse (1993), Variability of the tropical Atlantic ocean simulated by a general circulation model with two different mixed layer physics, *J. Phys. Oceanogr.*, *23*, 1363–1388, doi:10.1175/1520-0485(1993)023<1363:VOTTAO>2.0.CO;2.

Bopp, L., K. E. Kohfeld, C. Le Quéré, and O. Aumont (2003), Dust impact on marine biota and atmospheric pCO_2 during glacial periods, *Paleoceanography*, *18*(2), 1046, doi:10.1029/2002PA000810.

Boyd, P. W., et al. (1999), Transformations of biogenic particulates from the pelagic to the deep ocean realm, *Deep Sea Res., Part II*, *46*, 2761–2792, doi:10.1016/S0967-0645(99)00083-1.

Bradtmiller, L. I., R. F. Anderson, M. Q. Fleisher, and L. H. Burckle (2007), Opal burial in the equatorial Atlantic Ocean over the last 30 ka: Implications for glacial-interglacial changes in the ocean silicon cycle, *Paleoceanography*, *22*, PA4216, doi:10.1029/2007PA001443.

Brewer, P. G., Y. Nozaki, D. W. Spencer, and A. P. Fleer (1980), Sediment trap experiments in the deep North Atlantic: Isotopic and elemental fluxes, *J. Mar. Res.*, *38*, 703–728.

Charles, C., and R. Fairbanks (1992), Evidence from Southern-Ocean sediments for the effect of north Atlantic deep water flux on climate, *Nature*, *355*, 416–419, doi:10.1038/355416a0.

Chase, Z., and R. F. Anderson (2004), Comment on "On the importance of opal, carbonate, and lithogenic clays in the scavenging and fractioning ^{230}Th, ^{231}Pa and ^{10}Be in the ocean" by S. Luo and T. L. Ku, *Earth Planet. Sci. Lett.*, *220*, 213–222, doi:10.1016/S0012-821X(04)00028-7.

Chase, Z., R. F. Anderson, M. Q. Fleisher, and P. W. Kubik (2002), The influence of particle composition and particle flux on savenging of Th, Pa and Be in the ocean, *Earth Planet. Sci. Lett.*, *204*, 215–229, doi:10.1016/S0012-821X(02)00984-6.

Chase, Z., R. F. Anderson, M. Q. Fleisher, and P. W. Kubik (2003), Scavenging of 230Th, 231Pa and 10Be in the Southern Ocean (SW Pacific sector): The importance of particle flux, particle composition and advection, *Deep Sea Res., Part II*, *50*, 739–768, doi:10.1016/S0967-0645(02)00593-3.

Clegg, S. L., and M. Witfield (1991), A generalized model for the scavenging of trace metals in the open ocean_2 thorium

scavenging, *Deep-Sea Res.*, *38*, 91–120, doi:10.1016/0198-0149(91)90056-L.

Conkright, M., R. A. Locarnini, H. E. Garcia, T. D. O'Brien, T. P. Boyer, C. Stephens, and J. Antononov (2002), Objective analyses, data statistics and figures, technical report, NOAA, Silver Spring, Md.

Coppola, L., M. Roy-Barman, S. Mulsow, P. Povinec, and C. Jeandel (2006), Thorium isotopes as tracers of particles dynamics and deep water circulation in the Indian sector of the Southern Ocean (ANTARES IV), *Mar. Chem.*, *100*, 299–313, doi:10.1016/j.marchem.2005.10.019.

Curry, W. B., and D. W. Oppo (2005), Glacial water mass geometry and the distribution of δ C13 of Σ CO_2 in the western Atlantic Ocean, *Paleoceanography*, *20*, PA1017, doi:10.1029/2004PA001021.

Doney, S. C., et al. (2004), Evaluating global ocean carbon models: The importance of realistic physics, *Global Biogeochem. Cycles*, *18*, GB3017, doi:10.1029/2003GB002150.

Druffel, E. R. M., P. M. Williams, J. E. Bauer, and J. R. Ertel (1992), Cycling of dissolved and particulate organic matter in open ocean, *J. Geophys. Res.*, *97*, 15,639–15,659, doi:10.1029/92JC01511.

Duplessy, J. C., N. Shackelton, R. Fairbanks, L. Labeyrie, D. Oppo, and N. Kallel (1988), Deepwater source variations during the last climate cycle and their impact on the global deepwater circulation, *Paleoceanography*, *3*(3), 343–360.

Dutay, J.-C., et al. (2002), Evaluation of ocean model ventilation with CFC-11: Comparison of 13 global ocean models, *Ocean Modell.*, *4*, 89–120, doi:10.1016/S1463-5003(01)00013-0.

Dutay, J.-C., et al. (2004), Evaluation of OCMIP-2 Ocean Models Deep Circulation with Mantel Helium-3, *J. Mar. Syst.*, *48*, 15–36, doi:10.1016/j.jmarsys.2003.05.010.

Fichefet, T., and M. A. Morales Masqueda (1997), Sensitivity of a global sea ice model to the treatment of ice thermodynamics and dynamics, *J. Geophys. Res.*, *102*, 12,609–12,646, doi:10.1029/97JC00480.

Gehlen, M., L. Bopp, N. Ernprin, O. Aumont, C. Heinze, and O. Raguencau (2006), Reconciling surface ocean productivity, export fluxes and sediment composition in a global biogeochemical model, *Biogeosciences*, *3*, 521–537.

Gehlen, M., L. Bopp, N. Ernprin, O. Aumont, C. Heinze, and O. Raguencau (2006), Reconciling surface ocean productivity, export fluxes and sediment composition in a global biogeochemical model, *Biogeosciences*, *3*, 521–537.

Gent, P. R., and J. C. McWilliams (1990), Isopycnal mixing in ocean circulation models, *J. Phys. Oceanogr.*, *20*, 150–155, doi:10.1175/1520-0485(1990)020<0150:IMIOCM>2.0.CO;2.

Gherardi, J.-M., L. Labeyrie, J. McManus, R. Francois, L. Skinner, and E. Cortijo (2005), Evidence from the Northeastern Atlantic basin for variability in the rate of the meridional overturning circulation through the last deglaciation, *Earth Planet. Sci. Lett.*, *240*, 710–723, doi:10.1016/j.epsl.2005.09.061.

Guo, L., M. Chen, and C. Gueguen (2002), Control of Pa/Th ratio by particulate chemical composition in the ocean, *Geophys. Res. Lett.*, *29*(20), 1961, doi:10.1029/2002GL015666.

Heinze, C., M. Gehlen, and C. Land (2006), On the potential of Th-230, Pa-231, and Be-10 for marine rain ratio determinations: A modeling study, *Global Biogeochem. Cycles*, *20*, GB2018, doi:10.1029/2005GB002595.

Henderson, G. M., and R. F. Anderson (2003), The U-series toolbox for paleoceanography, *Rev. Mineral. Geochem.*, *52*, 493–531, doi:10.2113/0520493.

Henderson, G. M., C. Heinze, R. F. Anderson, and A. Winguth (1999), Global distribution of the ^{230}Th flux to ocean sediments constrained by GCM modelling, *Deep Sea Res., Part I*, *46*, 1861–1893, doi:10.1016/S0967-0637(99)00030-8.

Honeyman, B. D., et al. (1988), Oceanic trace metal scavenging: The importance of particle concentration, *Deep Sea Res.*, *35*, 227–246.

Jeandel, C., J. Bishop, and A. Zindler (1995), Exchange of Neodymium and its isotopes between seawater and small and large particles in the Sargasso Sea, *Geochim. Cosmochim. Acta*, *59*, 535–547, doi:10.1016/0016-7037(94)00367-U.

Kriest, I. (2002), Different parameterizations of marine snow in a 1D-model and their influence on representation of marine snow, nitrogen budget and sedimentation, *Deep Sea Res., Part I*, *49*, 2133–2162, doi:10.1016/S0967-0637(02)00127-9.

Kriest, I., and G. Evans (1999), Representing phytoplancton aggregates in biogeochemical models, *Deep Sea Res., Part I*, *46*, 1841–1859, doi:10.1016/S0967-0637(99)00032-1.

Krishnaswami, S., M. M. Sarin, and B. Somayajulu (1981), Chemical and radiochemical investigations of surface and deep particles of the Indian Ocean, *Earth Planet. Sci. Lett.*, *54*, 81–96, doi:10.1016/0012-821X(81)90071-6.

Kumar, N., R. Gwiazda, R. F. Anderson, and P. N. Froelich (1993), Pa-231/Th-230 ratios in sediments as a proxy for past changes in Southern Ocean productivity, *Nature*, *362*, 45–48, doi:10.1038/362045a0.

Kumar, N., R. F. Anderson, R. A. Mortlock, P. N. Froelich, P. Kubik, B. Dittrichhannen, and M. Suter (1995), Increased biological productivity and export production in the glacial Southern Ocean, *Nature*, *378*, 675–680, doi:10.1038/378675a0.

Lachkar, Z., J. C. Orr, J. C. Dutay, and P. Delecluse (2007), Effects of mesoscale eddies on global ocean distribution of CFC-11, $C0_2$ and Δ^{14}C, *Ocean Sci.*, *3*, 461–482.

Lea, D. (1995), A trace-metal perspective on the evolution of Antarctic circumpolar deep-water chemistry, *Paleoceanography*, *10*, 733–747, doi:10.1029/95PA01546.

Li, Y.-H. (2005), Controversy over the relationship between major components of sediment-trap material and the bulk distribution coefficients of ^{230}Th, ^{231}Pa, and ^{10}Be, *Earth Planet. Sci. Lett.*, *233*, 1–7, doi:10.1016/j.epsl.2005.02.023.

Loisel, H., et al. (2002), Seasonal and inter-annual variability of particulate organic matter in the global ocean, *Geophys. Res. Lett.*, *29*(24), 2196, doi:10.1029/2002GL015948.

Luo, S., and T.-L. Ku (1999), Oceanic 231Pa/230Th ratio influenced by particle composition and remineratisation, *Earth Planet. Sci. Lett.*, *167*, 183–199, doi:10.1016/S0012-821X(99)00035-7.

Luo, S., and T.-L. Ku (2004), On the importance of opal, carbonate, and lithogenic clays in the scavenging and fractioning ^{230}Th, ^{231}Pa and ^{10}Be in the ocean, *Earth Planet. Sci. Lett.*, *220*, 201–211, doi:10.1016/S0012-821X(04)00027-5.

Madec, G., P. Delecluse, M. Imbard, and C. Lévy (1998), OPA8.1 ocean general circulation model reference manual, *Notes Pôle Model. 11*, Inst. Pierre Simon Laplace, Paris.

Marchal, O., R. François, T. F. Stocker, and F. Joos (2000), Ocean thermohaline circulation and sedimentary ^{231}PA/^{230}Th ratio, *Paleoceanography*, *15*, 625–641, doi:10.1029/2000PA000496.

Marchal, O., R. Francois, and J. Scholten (2007), Contribution of Th-230 measurements to the estimation of the abyssal circulation, *Deep Sea Res., Part I*, *54*, 557–585, doi:10.1016/j.dsr.2007.01.002.

Matsumoto, K., et al. (2004), Evaluation of ocean carbon cycle models with data-based metrics, *Geophys. Res. Lett.*, *31*, L07303, doi:10.1029/2003GL018970.

McManus, G., R. Francois, J.-M. Gherardi, L. Keigwin, and S. Brown-Leger (2004), collapse and rapid resumption of

Atlantic meridional circulation linked to deglacial climate changes, *Nature*, *428*, 834–837, doi:10.1038/nature02494.

Moore, R., and K. Hunter (1985), Thorium adsorption in the ocean: Reversibility and distribution amongst particules sizes, *Geochim. Cosmochim. Acta*, *49*, 2253–2257, doi:10.1016/0016-7037(85)90225-X.

Moran, S. B., C.-C. Shen, S. E. Wienstein, L. H. Hettinger, J. A. Hoff, H. N. Edmonds, and R. L. Edwards (2001), Constrain on the deep water age and particle flux in the Equatorial and South Atlantic Ocean based on seawater 231Pa and 230Th data, *Geophys. Res. Lett.*, *28*, 3437–3440, doi:10.1029/2001GL013339.

Moran, S. B., C.-C. Shen, H. N. Edmonds, S. E. Weinstein, J. N. Smith, and R. L. Edwards (2002), Dissolved and particulate 231Pa and 230Th in the Atlantic Ocean: Constraints on intermediate/deep water age, boundary scavenging, and 231Pa/230Th fractionation, *Earth Planet. Sci. Lett.*, *203*, 999–1014, doi:10.1016/S0012-821X(02)00928-7.

Nozaki, Y., Y. Horibe, and H. Tsubota (1981), The water column distributions of thorium isotopes in the western North Pacific, *Earth Planet. Sci. Lett.*, *54*, 203–216, doi:10.1016/0012-821X(81)90004-2.

Rahmstorf, S. (2002), Ocean circulation and climate during the past 120,000 years, *Nature*, *419*, 207–214, doi:10.1038/nature01090.

Ridgwell, A. J., A. J. Watson, and D. E. Archer (2002), Modeling the response of the oceanic inventory to perturbation, and consequences for atmospheric CO_2, *Global Biogeochem. Cycles*, *16*(4), 1071, doi:10.1029/2002GB001877.

Roullet, G., and G. Madec (2000), Salt conservation, free surface and varying volume: A new formulation for Ocean GCMs, *J. Geophys. Res.*, *105*, 23,927–23,942, doi:10.1029/2000JC900089.

Roy-Barman, M., J. H. Chen, and G. J. Wasserburg (1996), ^{230}Th-^{232}Th systematics in the Central Pacific Ocean: The sources and the fates of thorium, *Earth Planet. Sci. Lett.*, *139*, 351–363, doi:10.1016/0012-821X(96)00017-9.

Roy-Barman, M., C. Jeandel, M. Souhaut, M. Van der Loeff, I. Voege, N. Leblond, and R. Freydier (2005), The influence of particle composition on thorium scavenging in the NE Atlantic ocean (POMME experiment), *Earth Planet. Sci. Lett.*, *240*, 681–693, doi:10.1016/j.epsl.2005.09.059.

Rutgers van der Loeff, M. M., and G. W. Berger (1993), Scavenging of 230Th and 231Pa near the Antarctic Polar Front in the South Atlantic, *Deep-Sea Res., Part 1*, *40*, 339–357, doi:10.1016/0967-0637(93)90007-P.

Santschi, P. H., J. W. Murray, M. Baskaran, C. R. Benitez-Nelson, L. D. Guo, C.-C. Hung, C. Lamborg, S. B. Moran, U. Passow, and M. Roy-Barman (2006), Thorium speciation in seawater, *Mar. Chem.*, *100*, 250–268.

Scholten, J., M. Vanderloeff, and A. Michel (1995), Distribution of Th-230 and Pa-231 in the water column in relation to the ventilation of the deep Arctic basins, *Deep Sea Res., Part II*, *42*, 1519–1531, doi:10.1016/0967-0645(95)00052-6.

Scholten, J. C., J. Fietzke, S. Vogler, M. M. Rutgers van der Loeff, A. Mangini, W. Koeve, J. Waniek, P. Stolers, A. Antia, and J. Kuss (2001), Trapping efficiencies of sediment traps from the deep Eastern North Atlantic: The 230Th calibration, *Deep Sea Res., Part II*, *48*, 2383–2408, doi:10.1016/S0967-0645(00)00176-4.

Scholten, J. C., et al. (2005), Radionucleide fluxes in the Arabian Sea: The role of particle composition, *Earth Planet. Sci. Lett.*, *230*, 319–337, doi:10.1016/j.epsl.2004.11.003.

Sherrell, R. M., M. P. Field, and Y. Gao (1998), Temporal variability of suspended mass and composition in the Northeast Pacific water column: Relationships to sinking flux and lateral advection, *Deep Sea Res., Part II*, *45*, 733–761, doi:10.1016/S0967-0645(97)00100-8.

Siddall, M., G. Henderson, N. Edwards, M. Frank, S. Muller, T. Stocker, and F. Joos (2005), Pa-231/Th-230 fractionation by ocean transport, biogenic particle flux and particle type, *Earth Planet. Sci. Lett.*, *237*, 135–155, doi:10.1016/j.epsl.2005.05.031.

Siddall, M., T. F. Stocker, G. M. Henderson, F. Joos, M. Frank, N. R. Edwards, S. F. Ritz, and S. A. Muller (2007), Modeling the relationship between ^{231}Pa/^{230}Th distribution in North Atlantic sediment and Atlantic merdional overturning circulation, *Paleoceanography*, *22*, PA2214, doi:10.1029/2006PA001358.

Spencer, D. (1984), *Global Ocean Flux Study*, 360 pp., Natl. Acad. Press, Washington, D. C.

Stemmann, L., G. Jackson, and D. Ianson (2004), A vertical model of particle size distributions and fluxes in the midwater column that includes biological and physical processes- Part I: Model formulation, *Deep Sea Res., Part I*, *51*, 865–884.

Thomas, A. L., G. M. Henderson, and L. F. Robinson (2006), Interpretation of the ^{231}Pa/^{230}Th paleocirculation proxy: New water-column measurements from the southwest Indian Ocean, *Earth Planet. Sci. Lett.*, *241*, 493–504, doi:10.1016/j.epsl.2005.11.031.

Timmermann, R., H. Goosse, G. Madec, T. Fichefet, C. Ethé, and V. Dulière (2005), On representation of high latitude processes in the ORCALIM global coupled sea ice-ocean model, *Ocean Modell.*, *8*, 175–201, doi:10.1016/j.ocemod.2003.12.009.

Tréguer, P., D. M. Nelson, S. Guenely, C. Zeyons, J. Morvan, and A. Buma (1990), The distribution of Biogenic and Lithogenic Silica and the composition of particulate organic-matter in the Scottia Sea and the Drake passage during Autumn 1987, *Deep Sea Res., Part A*, *37*, 833–851, doi:10.1016/0198-0149(90)90009-K.

Trimble, S. M., M. Baskaran, and D. Porcelli (2004), Scavenging of thorium isotopes in the Canada Basin of the Arctic Ocean, *Earth Planet. Sci. Lett.*, *222*, 915–932.

Venchiarutti, C., C. Jeandel, and M. Roy-Barman (2008), Particle dynamics in the wake of Kerguelen Island traced by thorium isotopes (Southern Ocean, KEOPS program), *Deep Sea Res., Part I*, *55*, 1343–1363.

Walter, H. J., et al. (2001), Shallow vs. deep-water scavenging of 231Pa and 230Th in radionuclide enriched waters of the Atlantic sector of the Southern Ocean, *Deep Sea Res.*, *48*, 471–493.

Yu, E. F., R. Francois, and M. P. Bacon (1996), similar rates of modern and last glacial ocean thermohaline circulation inferred from radiochemical data, *Nature*, *379*, 689–695, doi:10.1038/379689a0.